



UNIVERSITY  
OF ABERDEEN

ULTRASONIC TRACTOR BEAMS FOR PARTICLE  
MANIPULATION

NIALL MACDONALD  
2018

THIS THESIS WAS SUBMITTED AS PART OF THE REQUIREMENT FOR  
THE MENG DEGREE IN CHEMICAL ENGINEERING.

## ABSTRACT

This thesis summarises the background theory of acoustic levitation and discusses the importance of this emerging technology. The different devices that can produce acoustic traps are discussed with a single and double-sided ultrasonic transducer array built to test this technology physically. Python is used to program a model for the simulation of the acoustic fields produced by these devices and an algorithm developed to characterise the acoustic traps these fields produce. The design of the single-sided acoustic levitation device is improved over previous designs as it has a much greater ability to control the phases of each transducer individually, up to  $\pi/1250$ , by the use of a field programmable gate array (FPGA), to control the transducers. The optimisation of the parameters that affect the acoustic trap's strength are investigated and it is found that array power and array layout is vital to achieve optimal trap strength. It is also proven that acoustic traps formed by multi-sided arrays can be two orders of magnitude stronger than those that single-sided arrays produce. This improvement allows for the levitation of liquids and even some metals with optimal array layouts.

## ACKNOWLEDGEMENTS

I would first and foremost like to thank Dr Marcus Campbell Bannerman for his continuous support during this project. His passion and dedication is inspiring, and his work on the design and construction of the acoustic array is very much appreciated. His help in improving my software development skills was vital to the success of this project.

I would also like to thank Asier Marzo from the University of Bristol for the use of his open source acoustic trapping software "Ultraino" and for help with troubleshooting our array.

I would also like to thank Richard Osborne for all his support in the lab and for the use of his 3D printer.

# CONTENTS

<b>Abstract</b>	<b>2</b>
<b>Acknowledgements</b>	<b>2</b>
<b>1 Introduction</b>	<b>4</b>
<b>2 Sound Waves</b>	<b>7</b>
2.1 Ultrasound . . . . .	8
2.2 Complex Wave Representation . . . . .	9
2.3 Complex Acoustic Pressure . . . . .	9
2.4 Sound Wave Interactions . . . . .	11
<b>3 Ultrasonic Acoustic Levitation</b>	<b>13</b>
3.1 Acoustic Radiation Force . . . . .	13
3.2 Gor'kov Potential . . . . .	13
3.3 Acoustic Traps . . . . .	16
<b>4 Phased Array Design and Construction</b>	<b>24</b>
<b>5 Simulation of Acoustic Fields</b>	<b>30</b>
5.1 Acoustic Model Calibration . . . . .	30
5.2 Acoustic Trap Characterisation . . . . .	33
5.3 Acoustic Array Optimisation . . . . .	37
5.4 Particle Simulation . . . . .	43
<b>6 Conclusions and Future Work</b>	<b>45</b>
<b>7 References</b>	<b>47</b>

---

CHAPTER  
**ONE**

---

## INTRODUCTION

Particle manipulation is an essential technology for modern life. The production of food, pharmaceuticals, even soap involves some form of solids processing either in the powdered feedstocks or the solid catalyst beads used to process them. Efficient and effective transportation of these solids to where they are required is vital to the smooth operation of these processes.

Manipulation of individual particles in solids processing devices such as optical tweezers is a well-proven technology; they use a focused beam of laser light to trap particles in the order of micrometres. The force that holds the particle at this focus point is created by the change in momentum of light as it is reflected off and refracted through a microsphere. When the particle is in the centre of the trap, all the forces on it sum to zero, causing the particle to be stationary at that point. If the particle deviates from the centre, there is a net force on the particle towards the focus' centre. Therefore, the trap is stable as any deviation from the trap will restore the particle to its centre. Optical tweezers have been used as far back as the 1980s [1] to trap individual biological molecules and measure the forces exerted by them.

Acoustic tweezers are a new progression of this technology using ultrasonic transducers and sound wave interactions to create the trapping forces required to hold particles in place. The complexity of these systems has rapidly been progressing from standing wave stationary traps to controlled moving levitated objects in 2013 [2]. The technology has

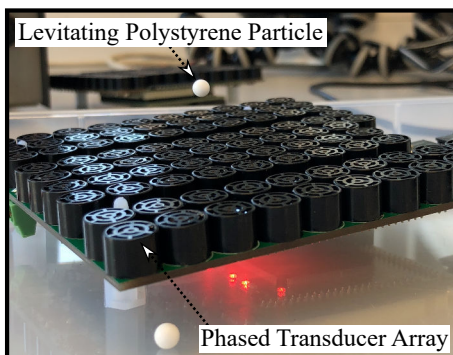


Figure 1.1: Phased array of 88 transducers levitating a 4.2 mm polystyrene sphere 2 cm above the array.

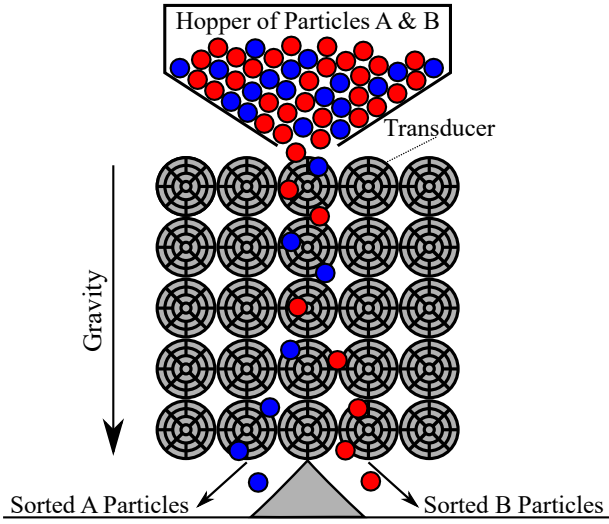


Figure 1.2: Vertical sorting mechanism which would separate a hopper of mixed particles into two distinct groups based on some predefined particle properties using directed ultrasonic traps.

advanced to the stage where a single-sided array of transducers can be controlled to hold and manipulate a particle in three dimensions, which was accomplished as recently as 2015 [3]. Real-time phase shift calculations are possible by the implementation of holographic phase elements [4] that are added to a calculated focusing phase pattern, to create acoustic traps at the desired locations. This allows the trap locations to be re-calculated in real-time and for the manipulation of particles in 3D space. It's also possible to hold particles with a diameter many times the wavelength using standing waves from multiple large transducers [5].

The principle behind the formation of the acoustic traps relies on the focusing of many sound signals by delaying them from their sources. This delay can be introduced electronically with computer controlled signal delays, with physical separation, with sculpted surfaces or with coiled delay lines [6]. The electronically controlled devices use a flat phased array of transducers shown in Figure 1.1. These phased arrays consist of many individually controllable ultrasonic transducers that can delay their sound signals by  $2\pi/1250$  radians from each other.

As the field is so new, there are many novel applications that are being explored for acoustic levitation devices. Currently, there are no commercial acoustic levitation devices available for sale, most of the devices are being built by universities for research into the technology. The applications include particle manipulation without physical touch; this could be useful for moving delicate samples of varying sizes [7] or dangerous materials through a medium without contact with anything else [2] [8]. Another exciting application is particle sorting; this could be accomplished by deflecting particles with specific properties in different directions, which would require computer vision and image recognition to detect the particles that are to be sorted. An example of what a basic sorting mechanism would look like is shown in Figure 1.2. The medical applications of this technology could be critical as the device would allow for targeted manipulation of particles

or drugs inside the body, without having to make surgical incisions [9].

Ultrasonic transducer arrays, similar to the array shown in Figure 1.1, have been used in many varied applications, for example, commercial ultrasound machines used for fetal imaging. These devices have been around since the 1950s and use ultrasonic transducers to output a signal and then the same transducers to listen for the echo of the sound from inside the body. This live 3D imaging requires complicated and expensive electronics to take analogue sound signals from the transducers and convert them into digital signals which the computer turns into 3D images.

Haptic Feedback is another application of phased acoustic arrays. Using ultrasound that is focused to a point then modulated at a frequency of around 200 Hz, it has been demonstrated that this is able to form a focus point in the air which can be felt by receptors in the human skin [10]. This technology has seen commercial development from companies such as UltraHaptics who have demonstrated that haptic feedback can be used to give tactile feedback to interactions with a computer through a screen [11]. It is also possible to direct audible sound to specific points using focused modulated ultrasonic waves [12], this makes use of the sound from ultrasound effect. Consequently, music or messages can be projected to a specific point in a room which is otherwise silent.

Ultrasonic waves have also been demonstrated to be able to power devices wirelessly by focusing a beam of ultrasound from a powered array to another non-powered array. The induced vibrations in the non-powered transducers convert the kinetic energy of the oscillating air into electrical power [13]. This allows devices which are not connected to a power source to be powered remotely.

This thesis explores phased arrays, and will introduce the underlying theory of sound and the acoustic radiation force which allows for the development of a theoretical model to predict the forces on particles in an acoustic potential field. This model is used in conjunction with basic particle simulation to allow for the investigation of different traps within a simulation of the acoustic field. To investigate this technology physically requires the design, manufacture and construction of an acoustic levitation device and the implementation of appropriate control software for that device.

The simulation parameters are calibrated using experiments, allowing accurate comparison between different acoustic trap types and trap locations over the array. The validation of the model enables rapid optimisation of the field without manual testing.

A second array is built and is used to form stronger trapping forces with a two-sided array, this allows for the trapping of liquids [14] which leads to the ability to measure properties such as the diffusion coefficients of different liquids. In the future this could allow for spectroscopy to be performed on a sample without contact with a container, meaning less interference in the readings.

Initially, the basic theory of sound is investigated allowing for a greater understanding of the underlying principles of acoustic levitation and how sound waves and sound pressure directly relate to acoustic levitation.

---

CHAPTER  
**TWO**

---

## SOUND WAVES

To understand how acoustic levitation is possible and why it works, it is first imperative to learn what sound is and how it propagates through different materials.

Sound can be characterised as an oscillation of pressure in some form of matter, either solid, gas, liquid, or plasma; this is usually called the medium. From a fixed point in space, if the sound source is stationary in relation to that point, the sound will appear as oscillations of pressure above and below the ambient pressure. Sound sources are usually vibrating objects, in the case of transducers, a small metal plate that vibrates back and forth causing the air in front of it to be compressed and expanded as the plate moves.

The sound propagates away from the source as a longitudinal wave at the speed of sound. A longitudinal wave is defined as the displacement of the medium in either the same direction as the sound wave or in the opposite direction. To visualise this type of wave it is like pushing a stretched slinky along its central axis; the coils will move away from the direction of force and then back again. The speed of sound is dependant on the medium that the sound is travelling through. The Newton-Laplace equation given as  $c = \sqrt{\frac{K}{\rho}}$  with  $c$  = the speed of sound,  $K$  = the elastic bulk modulus and  $\rho$  = the density of the medium. The speed of sound is thus shown to be dependant on the density of the medium and the elastic bulk modulus. The elastic bulk modulus is a thermodynamic property which means it is dependant on temperature. Therefore, the speed a sound wave will move through a medium is dependant on the ambient conditions as well as the material itself, for example in air at 20 °C the speed of sound is 343 m/s, and at 40 °C the speed of sound is 354 m/s. This is, therefore, a non-trivial dependence on temperature as the speed of sound changes by roughly 10 m/s with a temperature increase of 20 °C.

Sound waves do not carry the medium's molecules with it when it propagates. The time-averaged position of the medium's molecules will not move in space with the propagation of the sound waves. This is easy to visualise when looking at solids as they can transmit sound just like liquids and gases but their molecules are held in position.

Sound, just like any wave, has a phase which is the offset from the arbitrary start point of the wave. The full time it takes a wave to repeat back to its initial position is called the period of the wave. If a wave is offset by a full period, it is back where it started

and is indistinguishable from the non-offset wave. Shown in Figure 2.1 is a sine wave and another sine wave that has been offset by  $+\pi/2$ . This demonstrates the shift in time, or in space that waves can have as they leave the sound source. With transducers, it is possible to set this relative delay in relation to other transducers to form focus points and acoustic traps in the air. The acoustic levitation devices that have been constructed thus far have all used ultrasonic transducers as their sound sources. To understand why this choice is made and what the limitations and benefits of using ultrasound are, the topic is investigated further.

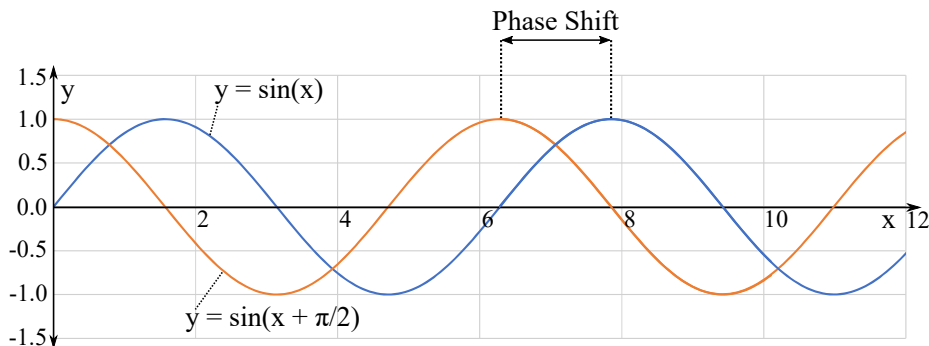


Figure 2.1: Graph of two sine waves showing the phase shift between them.

## 2.1 Ultrasound

Ultrasound is sound that is above the average human hearing frequency range of 20 Hz to 20 kHz. The reason that ultrasound and therefore ultrasonic transducers are selected for research into acoustic levitation technology is mainly a factor of cost. Small ultrasonic transducers are readily available in large, inexpensive quantities, which keeps the costs down as a substantial number of transducers are required in the arrays. Size is also a major factor in selecting ultrasound. Since the size of the particles that can be levitated is proportional to the wavelength of the sound waves, to have a practically sized device with particles in the 4 mm size range the sound needs to have a comparable wavelength. It has been shown that particles which are larger in diameter than half the wavelength of the sound are unstable in acoustic traps [15]. Most small ultrasonic transducers have an optimum operating frequency around 40 kHz. Using these transducers in air at 20 °C which has a speed of sound of 343 m/s, using the equation for wavelength: Wavelength = Speed of Sound / Frequency, a wavelength of  $\approx 8.6$  mm is found. Therefore particles below 4.3 mm will be stable.

It is essential to be able to represent these sound signals mathematically so they can be used in simulations and manipulated with equations. This representation needs to take into account the oscillatory behaviour of the sound waves and fully capture the vital information about these waves.

## 2.2 Complex Wave Representation

Since sound is a wave and is a function of time and position, to represent it mathematically a periodic function is required. Looking at the same point in space as the wave passes over will show an oscillating function. These types of functions can be described by sine and cosine functions. This is similar to simple harmonic motion where a wave passes over a point in space and the amplitude oscillates from the minimum to the maximum amplitude of the wave.

To represent sound, amplitude and phase components are required. To capture these two parts of the wave in one value, complex numbers are used, where the magnitude of the complex number represents the amplitude of the wave and the phase of the wave is represented by the angle of the complex number to the positive x-axis between 0 and  $2\pi$ .

Using Euler's formula Eq. 2.2.1, the sine and cosine components of an oscillating complex number can be represented by powers of the exponential function instead of real and imaginary trigonometric functions.

$$e^{ix} = \cos(x) + i\sin(x) \quad (2.2.1)$$

Using this representation of sound as complex powers of the exponential function, allows the calculation of the complex acoustic pressure at points in space. The pressure is a measure of how "loud" the sound is at that location; loudness is a subjective human perception of the sound pressure. Since human hearing does not have a linear response, our hearing ranges from as quiet as  $20 \mu\text{Pa}$  [16] to that of a jet engine from 1 meter away which has a sound pressure of around 650 Pa. Anything higher than this will cause serious discomfort and eventually permanent hearing damage. With human hearing having such a large range, a logarithmic scale is used to represent the very small numbers along with the very large numbers in a reasonable way. This scale is called the decibel scale where a reference sound level, usually the threshold of human hearing at  $20 \mu\text{Pa}$  is set as zero, giving the decibel as  $\text{dB} = 20 \log_{10}(\text{power}/\text{reference power})$ . Therefore 0 dB is no audible sound and 150 dB is a jet engine from 1 meter away.

## 2.3 Complex Acoustic Pressure

To determine the complex acoustic pressure at each point in space, a model for how sound disperses in a medium is needed. The acoustic field can be experimentally measured by using a transducer and scanning the field while recording the amplitude and phase of the waves at that point. To model the process in a practical way, an analytical model to represent the field is essential. A reasonably simple method exists for calculating this acoustic pressure using a far field piston model [3] [17]. The complex acoustic pressure  $P(r)$  at some point  $\vec{r}$  is given by Eq. 2.3.1:

$$P(r) = p_0 A \frac{D_f(\theta)}{d} e^{i(\varphi + k d)} \quad (2.3.1)$$

With  $p_0$  as a constant dependant on the transducers output power and  $A$  as the peak to peak amplitude of the transmitted signal. The propagation distance in free space  $d$ , the initial phase of the transmitting transducer as  $\varphi$ .  $k$  being the wave number given as  $k = 2\pi/\lambda$  with  $\lambda$  as the wavelength of the sound signal and  $D_f(\theta)$  which is a function that takes into account the directionality of the output of the transducer, since being directly above the transducer would give a larger pressure than at 90 degrees. This term can be simplified to  $D_f(\theta) = \text{sinc}(ka \sin(\theta))$  where  $a$  is the radius of the transducer and  $\text{sinc}(x) = \frac{\sin(x)}{x}$ . The propagation distance in free space term is written as  $1/d$  which means the acoustic pressure decreases proportionally to,  $1/d$ . This is derived from the fact that sound intensity decreases as  $1/d^2$  from its source [18]. Sound intensity is defined as  $I = pv$  where  $I$  is the sound intensity in  $\text{W/m}^2$ ,  $p$  is the sound pressure and  $v$  is the particle velocity. Since sound intensity is sound power per square meter, directionality function used in then it can be written as  $I = P/A(r)$ , for a point source spherical sound wave  $I = P/(4\pi r^2)$ . Therefore the sound intensity at a point  $r$  is proportional to  $1/r^2$ . This demonstrates that sound intensity follows the inverse square law for a spherical sound wave.

The transducer directionality function used in the acoustic pressure calculation is visualised below in Figure 2.2. This function takes into account the decreased sound pressure felt off axis to the normal of the transducer. The experimental directionality function taken from the transducer data sheet of Ref. [19] is shown at the left of Figure 2.2 as a comparison between the real directionality function and its simplification.

This acoustic pressure at each point in space is for a single transducer. To get the total pressure and final phase at each location if multiple transducers are used, the complex pressure contributions from each can be added together. Such that  $P(r)_{total} = \sum_{j=1}^n P(r)^j$ .

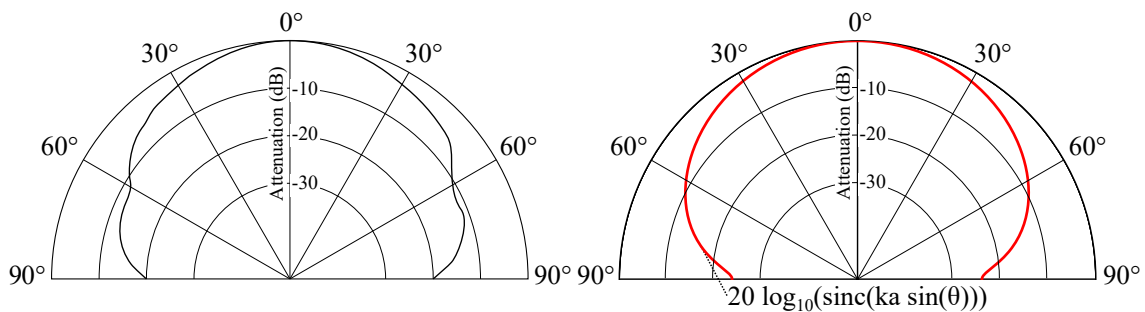


Figure 2.2: Experimental directionality function of Transducer MA40S4S (left), taken from transducer data sheet [19], and a Polar Plot of the simplified directionality function (right). These transducers are 40kHz transducers, similar to the ones used in the array board. The plot shows the proportional difference in decibels between different angles and how at extreme angles to the transducer's normal, the power drops off significantly.

When multiple sound waves overlap and come into contact with each other, like the two-phase shifted sine waves from Figure 2.1, there are interactions between those waves, and they create new waves in the process. These interactions are vital to understanding how acoustic traps are created.

## 2.4 Sound Wave Interactions

The acoustic field is hard to visualise as it changes with time and with space. As the sound waves move through the air, just like waves in a pond, they propagate out from the source, decreasing in intensity as they lose energy to frictional and other losses. A transducer that is continually outputting an oscillating signal would not diminish with time like a wave created by a pebble in a pond would. Instead, the waves would be strongest closest to the transducer and diminish as you move further away, all while oscillating above and below the ambient pressure.

As shown in Figure 2.3 the two sine waves are slightly out of phase and when they combine they constructively add to form a new wave, shown in green, which has a higher amplitude than either of the original waves had. Shown in Figure 2.4 are two sine waves that are  $\pi$  out of phase from each other; they destructively interfere and entirely cancel to form no wave. This shows that by controlling the phase shifts of multiple sound signals, selective constructive and destructive interference can be achieved. This principle is how active noise cancelling headphones work, by listening for sounds with a microphone and then playing the inverse of the sound to cancel the unwanted sound waves.

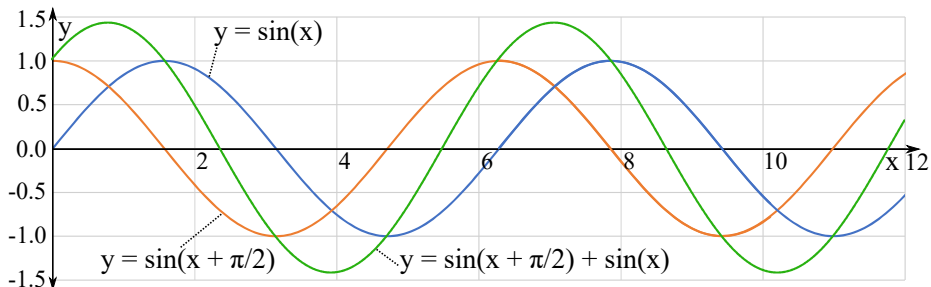


Figure 2.3: Graph of two sine waves (Blue and Orange) adding constructively to form a new wave (Green).

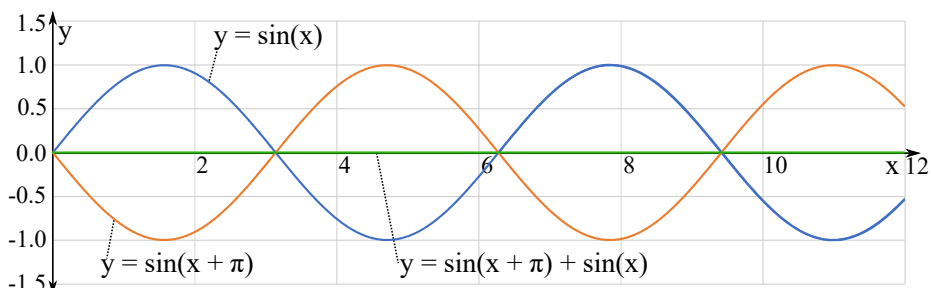


Figure 2.4: Graph of two sine waves (Blue and Orange) adding destructively to form a new wave (Green).

To visualise the acoustic pressure field, a time-averaged function for the acoustic pressure due to a piston source is used, given in Eq. 2.3.1. Shown on the right side of Figure 2.5 is a single transducer outputting a signal and the acoustic pressure field it creates in 3D. It shows, with the aid of iso-pressure shells, that as you move away from the transducer,

the magnitude of the complex pressure decreases and eventually becomes undetectable. The simulation ignores reflections, other interferences and any non-linear effects [4].

When there are multiple sources of sound, the waves created by each will interact with each other. Multiple waves will add together if they meet at the same point in space. Waves will add to become larger if they are in phase with each other, e.g. if both waves have positive or, both have negative phases. This is constructive interference as the combined wave becomes larger than either wave was alone. The inverse of this is destructive interference when the waves have opposite signs of their phases and when they add together, they become smaller. If the phases were exactly opposite, e.g. a peak of one wave meeting the trough of another and they had the same amplitude then they would entirely cancel out creating a region of no sound pressure. Shown on the left side of Figure 2.5 is the acoustic field that is created by the interactions of two transducers outputting the same signal at the same initial phase. The constructive and destructive interference effects are visible compared to the single transducer field on the right.

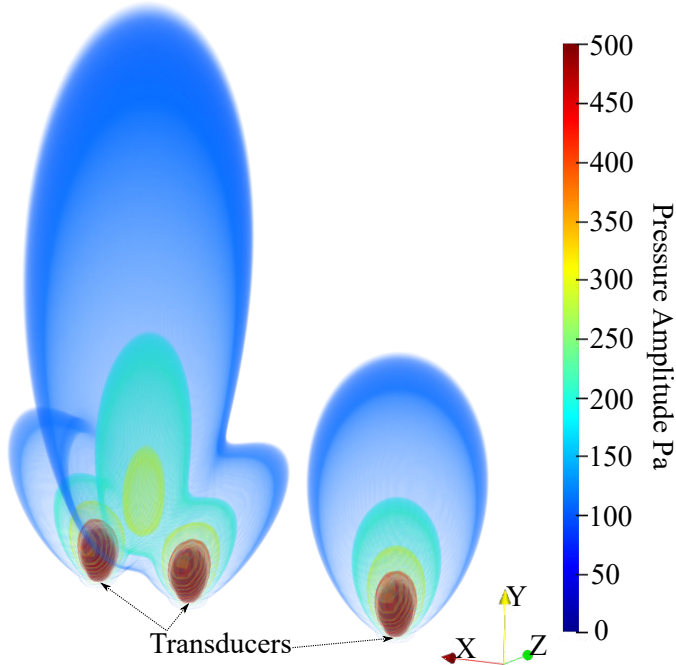


Figure 2.5: 3D plot of two separate simulations showing the absolute value of the complex acoustic pressure with two transducers on the left and one on the right. The plot shows iso-pressure shells of a single value to show the shape of the acoustic field in 3D. The plots are not scaled so the relative sizes between the two can be compared. In the left simulation, the transducers are in phase and are separated by 1 cm.

Using this property of wave addition allows the combination of many sound sources to form regions of space with low pressure surrounded by regions of high-pressure. This is essentially an acoustic trap, but to understand how these are formed and how they can be calculated, the acoustic potential field needs to be defined. This field is used in the calculation of the forces on particles and is discussed further in the following chapter.

---

CHAPTER  
**THREE**

---

## ULTRASONIC ACOUSTIC LEVITATION

### 3.1 Acoustic Radiation Force

The acoustic radiation force was first modelled by King in 1934 [20]. Comparable to how force is generated with electromagnetic waves in optical tweezers, the acoustic radiation force is formed from the change in momentum of the air particles as they are reflected off the levitated particle's surface. These scattering wave forces were derived in detail by Bruus in 2012 [21]. The sound waves approach the particle from a specific direction, this causes one side of the particle to receive more reflections than the other. These unbalanced forces cause the particle to be accelerated in the direction of the force.

This force can be calculated as the negative gradient of the acoustic potential  $U$ .

$$F = -\nabla U \tag{3.1.1}$$

This is comparable to gravitational potential energy as the force due to gravity is always towards the lower potential state, or downwards. This is the same as the negative gradient of the gravitational potential energy since the gradient always points uphill. An expression for the acoustic potential is therefore required to be able to calculate these forces. Lev Petrovich Gor'kov was the first to simplify a solution to calculate the acoustic potential field from any arbitrary complex acoustic pressure field [22].

### 3.2 Gor'kov Potential

The Gor'kov potential is a simplification of the acoustic potential field that is used to calculate the forces on particles that are smaller than the wavelength of the sound. It was generalised and summarised by Lev Petrovich Gor'kov in 1962 [22] and then later fully derived by Bruus in 2012 [21] and in standing wave fields by Barmatz et al. [23]. A convenient way to present this potential field is in terms of the acoustic pressure at that point in space. Rearranged by Asier Marzo in terms of pressure [4] the Gor'kov potential  $U$  is given by:

$$U = 2 K_1 (|P|^2) - 2 K_2 (|P_x|^2 + |P_y|^2 + |P_z|^2) \quad (3.2.1)$$

$$k_1 = \frac{1}{4} V \left( \frac{1}{c_0^2 \rho_0} - \frac{1}{c_s^2 \rho_s} \right)$$

$$k_2 = \frac{3}{4} V \left( \frac{\rho_0 - \rho_s}{\omega^2 \rho_0 (\rho_0 + 2 \rho_s)} \right)$$

With  $V$  as the volume of the particle,  $\omega$  as the frequency of the sound waves (40 kHz for the ultrasonic transducers). The subscripts 0 and  $s$  represent the air and the particle respectively.  $\rho$  is the density,  $c$  is the speed of sound and  $P$  is the complex acoustic pressure (expressed in the previous section). The complex pressures with subscripts  $P_x$ ,  $P_y$  and  $P_z$ , are the spatial derivatives of the complex pressure in those three directions x, y and z respectively.

This equation cannot be directly solved for a point in space, as the spatial derivatives of pressure are required. These can be calculated numerically by calculating the pressure function at small distances either side of the required point, and performing a numerical differentiation. This method is not particularly useful as it cannot reliably be used in optimisers and it also introduces large errors. This is not just estimation errors directly from the numerical differentiation methods, but as the numbers involved are very small, this causes problems with representation error when taking away very small numbers from comparably large numbers (even with 64-bit floating point numbers). An analytical expression for the derivative of the complex pressure with respect to  $\vec{r} = [x, y, z]$  is therefore desirable.

Defining the transducer position in space as  $\vec{r}_t = [x_{T_{pos}}, y_{T_{pos}}, z_{T_{pos}}]$ , the direction of the transducer normal as  $\vec{n}_t = [x_{dir}, y_{dir}, z_{dir}]$  and the point in space as  $\vec{r} = [x, y, z]$ .

The separation vector between the transducer and the point in space is defined as:

$$\vec{r}_s = \vec{r} - \vec{r}_t$$

The distance  $d(r)$  between the transducer and the point in space is the magnitude of the separation vector:

$$d(r) = |\vec{r}_s| = \sqrt{\vec{r}_s^2}$$

The angle  $\theta$  between the transducer normal  $\vec{n}_t$  and the point in space  $\vec{r}$  is:

$$\theta = \arccos \left( (\vec{r}_s \cdot \vec{n}_t) / |\vec{r}_s| \right) \quad \text{more usefully written as} \quad \sin(\theta) = \sqrt{1 - \left( (\vec{r}_s \cdot \vec{n}_t) / |\vec{r}_s| \right)^2}$$

Substituting the equation for  $D_f(\theta)$  and  $d(r)$  into Eq. 2.3.1 the complex pressure at point  $\vec{r}$  is defined as:

$$P(r) = p_0 A \frac{\sin(k a \sin(\theta))}{|\vec{r}_s| k a \sin(\theta)} e^{i(\varphi + k |\vec{r}_s|)}$$

Rearranging, so taking the derivative is easier:

$$P(r) = \underbrace{\frac{p_0 A \sin(k a \sin(\theta))}{k a \sin(\theta)}}_{f_1} \underbrace{\frac{e^{i(\varphi + k |\vec{r}_s|)}}{|\vec{r}_s|}}_{f_2}$$

Taking the first derivative of  $P(r)$  with respect to  $\vec{r}$ :

$$\frac{dP(r)}{dr} = \left( \frac{df_1}{dr} f_2 \right) + \left( f_1 \frac{df_2}{dr} \right)$$

The derivative  $df_2/dr$  using the quotient rule is given by:

$$\begin{aligned} f_2 &= \frac{e^{i(\varphi+k|\vec{r}_s|)}}{|\vec{r}_s|} \Rightarrow \frac{f_3}{f_4} \\ \frac{df_2}{dr} &= \frac{\left( \frac{df_3}{dr} f_4 \right) - \left( f_3 \frac{df_4}{dr} \right)}{f_4^2} \\ \frac{df_2}{dr} &= \frac{\vec{r}_s i k e^{i(\varphi+k|\vec{r}_s|)}}{|\vec{r}_s|^2} - \frac{\vec{r}_s e^{i(\varphi+k|\vec{r}_s|)}}{|\vec{r}_s|^3} \end{aligned} \quad (3.2.2)$$

The derivative  $df_1/dr$  using the quotient rule is given by:

$$\begin{aligned} f_1 &= \frac{p_0 A \sin(k a \sin(\theta))}{k a \sin(\theta)} \Rightarrow \frac{f_5}{f_6} \\ \frac{df_1}{dr} &= \frac{\left( \frac{df_5}{dr} f_6 \right) - \left( f_5 \frac{df_6}{dr} \right)}{f_6^2} \end{aligned} \quad (3.2.3)$$

The derivative  $df_6/dr$  is given by:

$$\begin{aligned} \frac{df_6}{dr} &= \frac{d k a \sin(\theta)}{dr} = k a \frac{d \sin(\theta)}{dr} \\ \frac{d \sin(\theta)}{dr} &= \frac{-\frac{\vec{r}_s \cdot n_t}{|\vec{r}_s|}}{\sqrt{1 - \frac{\vec{r}_s \cdot n_t}{|\vec{r}_s|}}} \frac{(n_t \cdot |\vec{r}_s|) - \hat{r}_s(n_t \cdot r_s)}{|\vec{r}_s|^2} \quad \text{with} \quad \hat{r}_s = \frac{\vec{r}_s}{|\vec{r}_s|} \\ \frac{df_6}{dr} &= k a \frac{-\frac{\vec{r}_s \cdot n_t}{|\vec{r}_s|}}{\sqrt{1 - \frac{\vec{r}_s \cdot n_t}{|\vec{r}_s|}}} \frac{(n_t \cdot |\vec{r}_s|) - \hat{r}_s(n_t \cdot r_s)}{|\vec{r}_s|^2} \end{aligned} \quad (3.2.4)$$

The derivative  $df_5/dr$  is given by:

$$\frac{df_5}{dr} = \frac{d p_0 A \sin(k a \sin(\theta))}{dr} = p_0 A \frac{d \sin(k a \sin(\theta))}{dr}$$

$$\frac{df_5}{dr} = p_0 A \cos(k a \sin(\theta)) \frac{d k a \sin(\theta))}{dr} = p_0 A \cos(k a \sin(\theta)) \frac{df_6}{dr} \quad (3.2.5)$$

Therefore the full version of  $\frac{df_1}{dr}$  Eq. 3.2.3 can be found by substituting Eq. 3.2.4 and 3.2.5 into it. This equation becomes very large and is impractical to show.

Finally, all the terms of Eq. 3.2.6 are known and the full equation can be built from these terms.

$$\frac{dP(r)}{dr} = \left( \frac{df_1}{dr} f_2 \right) + \left( f_1 \frac{df_2}{dr} \right) \quad (3.2.6)$$

This equation is checked by solving this analytical derivative which takes in the initial phase of the transducer  $\varphi$ , the point in space  $\vec{r}$ , the position of the transducer  $\vec{r}_t$  and the direction of the transducer  $\vec{n}_t$ . It also requires all the constants described for Eq. 2.3.1. The function then outputs the three spatial derivatives  $P_x$ ,  $P_y$  and  $P_z$  as a vector. These were compared to the same positions calculated using numerical differentiation to test if the function was giving the correct differentials.

For example a point at  $\vec{r} = [0.5, 0.4, 0.4]$  with the transducer pointing straight up  $\vec{n}_t = [0, 0, 1]$  at the origin  $\vec{r}_t = [0, 0, 0]$  with the initial phase of the transducer being 0. The derivatives of  $P(r)$  with respect to x, y and z are shown in Table 3.1.

Table 3.1: Numerical and analytical derivatives to illustrate the validity of the analytical solution for the derivative of the acoustic pressure.

	Numerically	Analytically
<b>P_x</b>	-234.816 - 48.685j	-234.747 - 49.008j
<b>P_y</b>	-187.842 - 38.946j	-187.798 - 39.206j
<b>P_z</b>	-188.618 - 35.054j	-188.758 - 34.392j

This example shows that the analytical differentiation calculates the correct derivatives in all the spatial dimensions. The small differences are due to the errors discussed previously in the numerical methods. This expression is then used to directly calculate the derivative terms  $P_x$ ,  $P_y$  and  $P_z$  in the equation for the acoustic potential Eq. 3.2.1, therefore, eliminating the need for numerical differentiation completely. Finally, with an expression for the acoustic potential field, acoustic traps can be investigated as minima of this field.

### 3.3 Acoustic Traps

Acoustic traps are regions of space where a particle can be stably held in place without being touched by a physical object. Particles are held in an acoustic field that is created by an array of ultrasonic transducers and the force that holds the particles against gravity is called the acoustic radiation force represented by Eq. 3.1.1. If numerous transducers are

used and the phase delays of the transducers adjusted, different interference patterns can be created. Sound waves either interact constructively or destructively with each other producing higher amplitude waves where there is constructive interference, and lower amplitude waves where there is destructive interference. This interaction creates nodes (high amplitude) and anti-nodes (low amplitude) in the wave patterns. The phases of the transducers can be adjusted to form regions of low amplitude waves surrounded by high amplitude waves and with the correct particle size and material, this point can become a stable trap where the forces on the particle all converge towards its centre. This means any deviation from this point results in a restoring force that accelerates it back to the traps centre.

As a 2D example, one spatial dimension and one energy dimension, Figure 3.1 shows the relationship between the gradient of the potential energy field and the forces on the particles in them. The gradient always points uphill and the force on the object always points downhill, directly opposite to the gradient. A stable trap is a point where the gradient of  $U$  is zero and the gradients surrounding this point diverge (a minimum in  $U$ ) and therefore the forces on the particle converge. If the particle is displaced from this trap point, it will be restored to its initial position with a restoring force. The unstable trap is the opposite of this where the gradient of  $U$  is also zero, but the surrounding points have converging gradients which therefore means diverging forces. Any deviation from this point will cause the particle to be accelerated away from this trap point.

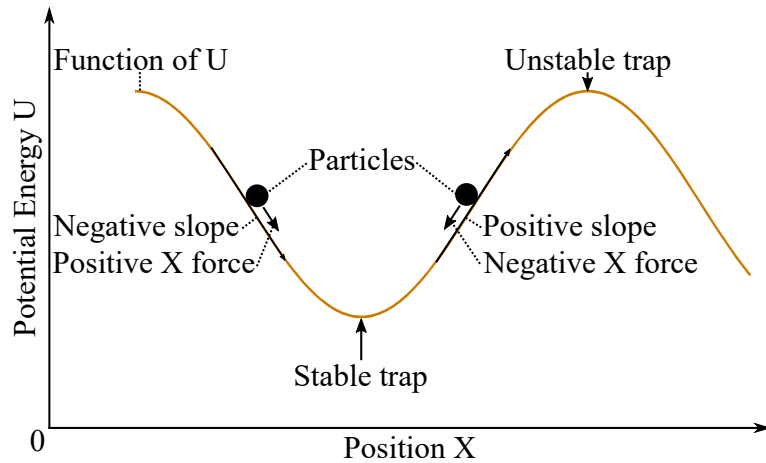


Figure 3.1: Graph of a function of potential energy analogous to the slopes of a hill with the particles rolling down them. This shows the opposite relationship between the slope of the potential field and the forces on the particles.

In three dimensions, the derivative of  $U$  at each point in space will give a vector that points in the direction of quickest increase of the function for  $U$ . Taking the derivative of this vector field would result in a new scalar field which gives negative values for maximums of  $U$  and positive numbers for minima of  $U$ . The magnitude of this second derivative of a scalar field is called the Laplacian and is denoted by  $\nabla^2$ . A maximum in potential energy, as shown in the unstable trap in Figure 3.1 gives negative Laplacian values and the steeper this maximum, the larger the negative Laplacian becomes.

Therefore the stable trap which has a minimum in potential energy will have positive values of the Laplacian. It is easy to compare different trap points with this number. As a larger Laplacian value will give a steeper trap (one where the gradients are larger on all sides of the minimum of U), bigger gradients mean the forces will also be bigger and therefore for the strongest trap point, a maximum in the Laplacian of U is desired  $\max\{\nabla^2 U\}$  [3]. This is comparable to the difference between a ball in a satellite dish or in a golf hole. It is easy to move a ball away from the minimum of a satellite dish, e.g. it takes a small amount of energy. The ball in the golf hole is much more stable at its minimum as it takes much more energy to move it out of its steep gradient trap point. It is therefore essential to be able to differentiate between a large trap volume with a slight energy difference like the satellite dish and a small trap volume with a steep energy difference like the golf hole.

Using this principle of maximising the Laplacian of U, it is possible to solve for the optimum transducer phase offsets, since the acoustic pressure with a fixed array and fixed location in space is only dependant on the initial phases of the transducers. Having a computer brute force the maximum Laplacian for all possible phase offsets for an array of any appreciable size is computationally prohibitive. An elegant solution to this problem was found by Asier Marzo allowing for the real-time calculation of the required phase offsets for optimal acoustic traps.

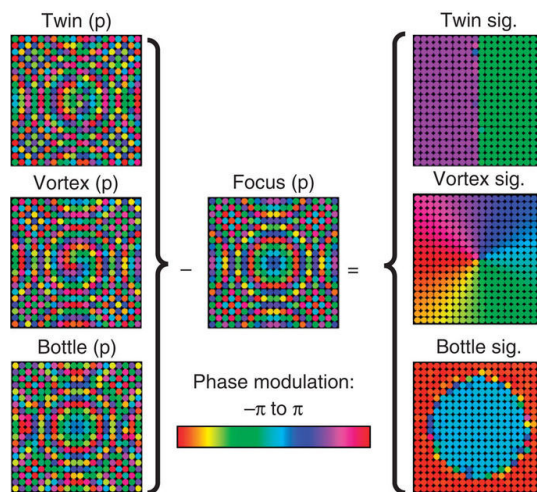


Figure 3.2: Figure of Ref. [3]: Phase modulations of the transducers for generating each of the acoustic traps (left), their decomposition into a focusing element (centre) and the holographic signatures (right).

Using holographic acoustic elements that have been shown to create optimal acoustic traps [3], it is possible to calculate the phase offsets of the transducers to create these traps in real-time. There are three holographic acoustic trap types that are either optimised around a plane of symmetry, a line of symmetry or a point of symmetry. These trap types have been named Twin Trap, Vortex Trap and Bottle Trap respectively. Shown in Figure 3.2 are 20 by 20 grids of transducers that show their phase offsets from each other by using colour. Adding the focus point to the acoustic signature, the trap signature can be

calculated, this is illustrated in the diagram which shows each trap types unique signature. The focus point is calculated by shifting the phases of the transducers depending on their distance from the trap point so that they all arrive at the focus point in phase.

To visualise these acoustic fields and therefore the traps, initially, the complex acoustic pressure is calculated using Eq. 2.3.1 in a grid layout of predetermined size with a  $\Delta X$  spacing in all three spatial dimensions. This creates a three-dimensional array of complex numbers which represents the complex acoustic pressure at those points. The Gor'kov potential can then be calculated in a grid, the same way as the complex acoustic pressure, using Eq. 3.2.1. This 3D scalar array can be visualised as a 3D array of point values that are coloured depending on their values. To visualise the forces a particle would experience in this potential field, the negative gradient of this potential is taken Eq. 3.1.1. This will produce a 3D array of vectors; this sort of data is tough to comprehend without visualisation software. These vectors can be rendered as arrows pointing in the direction of the vector and scaled in size or colour depending on their magnitude.

To illustrate these techniques, a field that has been proven to levitate particles up to a maximum of 4 mm by Asier [4] is rendered in 3D with two different views in Figure 3.3. This field shows the magnitude of the complex acoustic pressure scaled with colour and made partially transparent to allow the structures to become visible. It can be seen that the twin trap acoustic element creates a plane which the field is mirrored across. This plane can be rotated 360 degrees and allows for the two high-pressure bulbs to be rotated to any angle required. As discussed in the trap characterisation chapter, this property is useful as the trap is stronger in the direction of the bulbs and could be used to selectively move particles in one direction over another.

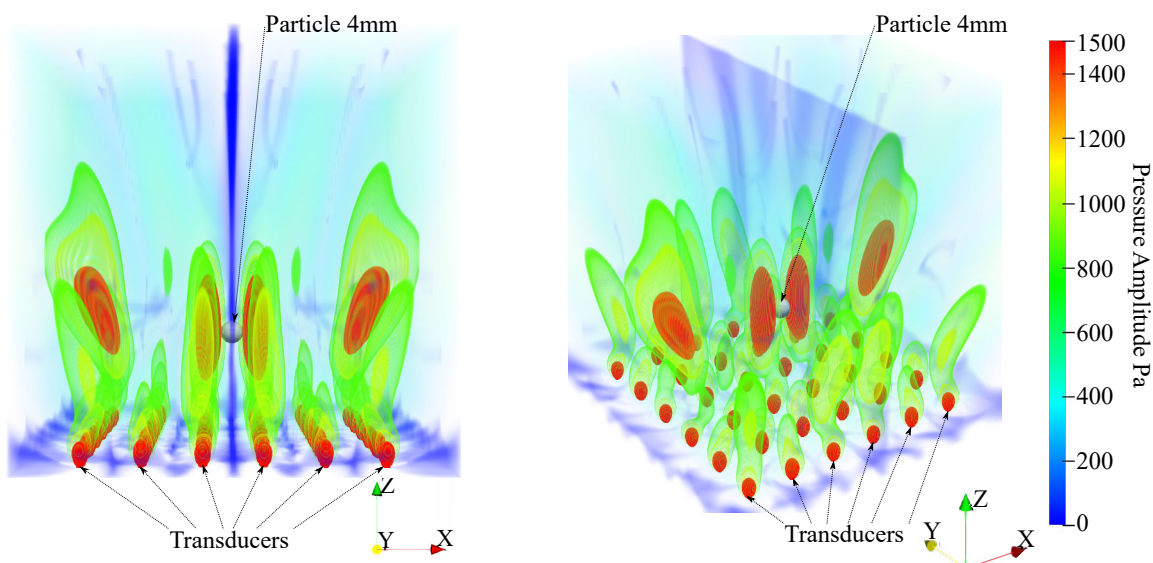


Figure 3.3: Two 3D plots showing the absolute value of the complex acoustic pressure for a twin trap acoustic element. Calculated with a 6 by 6 array of transducers separated by 1 cm in a square grid pattern. The plot shows iso-pressure shells to illustrate the shape of the acoustic field in 3D.

The acoustic potential field that this pressure field produces is shown in Figure 3.4. This potential field includes gravitational potential energy which can be seen as the steady increase of energy from the bottom to the top of the region box. Gravity is included as the acoustic field needs to hold the particle up against gravity, otherwise there would be no trap in reality. It can be seen that this potential field creates a minimum at the trap location which is in the same location as the particle shown in Figure 3.3. A minimum in energy is analogous to a valley, where a particle would fall towards the centre if it is inside the trap volume, and would be pushed away if it is on the outside.

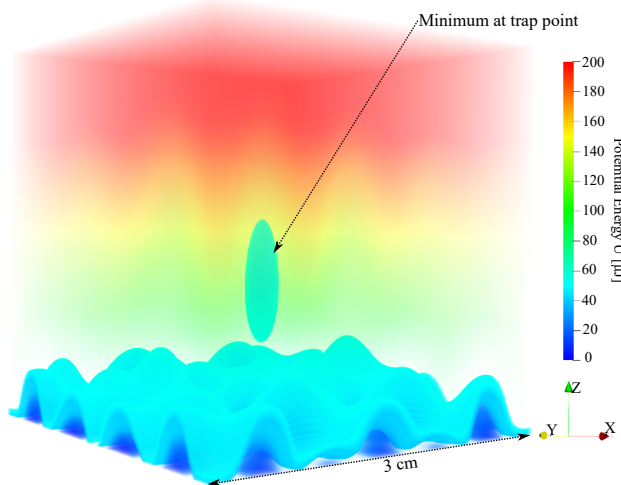


Figure 3.4: 3D plot showing the same field as in Figure 3.3 but displaying the acoustic potential  $U$  (including gravitational potential energy). Showing a 6 by 6 array of transducers separated by 1 m in a square grid pattern. The plot shows the shape of the acoustic potential field in 3D and clearly illustrates a minimum at the trap location.

The same technique is used to calculate the pressure field for the vortex trap which is shown in Figure 3.5. It can be seen that a line of symmetry is created and the trap is almost symmetrical around the shown central vertical line. A high-pressure torus is formed around the trap location which is symmetrical and its rotation does not affect trap strength. It is still possible to rotate this trap type in the same way as the twin trap. Using this technique with specially designed acoustic arrays that surround the particle, it is possible to trap particles larger than half the wavelength of the sound wave by inducing vortices and spinning the trap around the particle [24]. This was demonstrated as recently as January 2018 which shows the infancy of this research field.

This field produces a similar potential field to the one shown in Figure 3.4 where there is a minimum at the trap location and similar upwards gradient due to gravity. The differences between the trap types are discussed quantitatively in the acoustic trap characterisation section 5.2.

To demonstrate the bottle trap type, it is necessary to use a larger array as minima do not form on such small arrays, unlike the other two trap types. This is mainly due to the way the trap is formed as shown in Figure 3.2 without a significant number of transducers in both regions separated by a phase shift of  $\pi$ , the field that is formed does not produce

a stable trap point. The distance from the centre that the phase shift circle is calculated from can be adjusted to optimise the traps volume. This trap type theoretically can trap particles but has yet to be demonstrated in practice. The pressure field that this trap type produces is shown in Figure 3.6. It can be seen that it produces two high-pressure regions above and below the trap location and that the surrounding values are symmetrical, similar to the vortex trap. This trap type is a slight variation on the focus point and by focusing the inner part of the array precisely half out of phase with the outer part, it allows the interference pattern to cause a point of symmetry where there is a pressure minimum at the trap location in all three spatial dimensions.

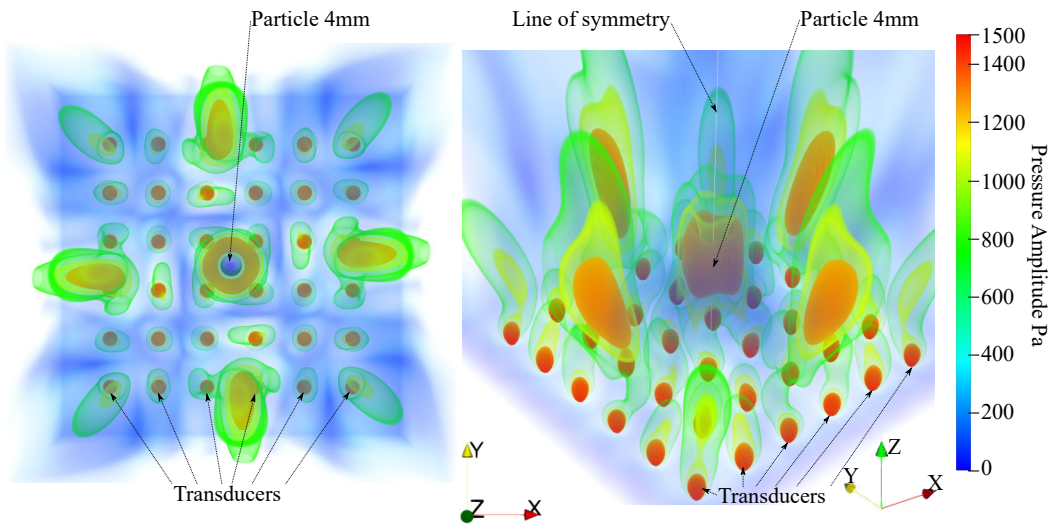


Figure 3.5: Two 3D plots, from above on the left and isometrically on the right, showing the absolute value of the complex acoustic pressure for a vortex trap. Calculated with a 6 by 6 array of transducers separated by 1 cm in a square grid pattern. The plot shows iso-pressure shells to illustrate the shape of the acoustic field in 3D.

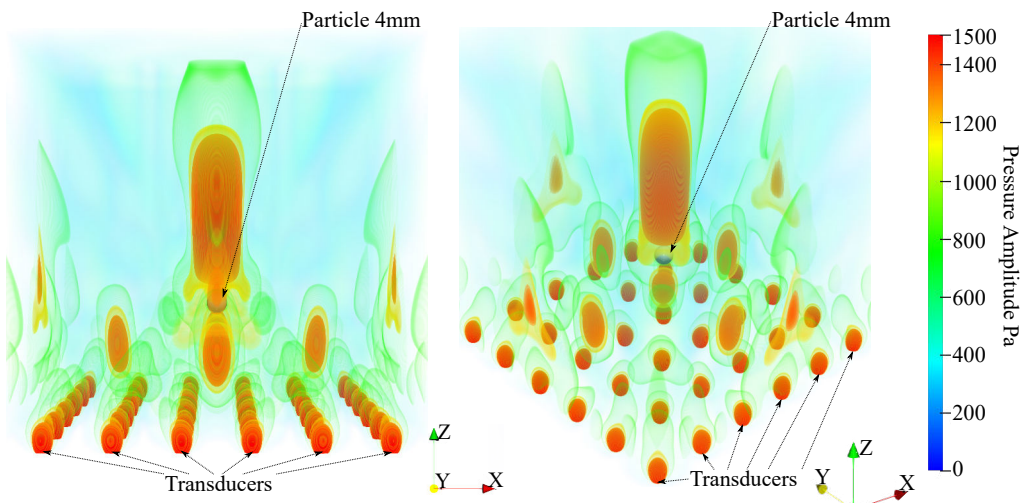


Figure 3.6: Two 3D plots, from the side on the left and isometrically on the right, showing the absolute value of the complex acoustic pressure for a bottle trap. Calculated with an 8 by 8 array of transducers separated by 1 cm in a square grid pattern, not all transducers are visible in the calculated boundary.

The above examples all use single-sided acoustic arrays; these have limited ability to trap particles due to their one-sided nature. The reason that these traps can be created with single-sided arrays is that the trapped particle is sufficiently close to the array that the external transducers appear to the particle as if they are to the side of them, therefore the angle between the outer transducer's normal and the particle is large. These arrays have been shown to create stronger traps by using a reflector as an acoustic mirror which creates standing wave, acoustic traps [25]. The flat array traps as discussed later are weaker than traps formed by two or more arrays at different angles to the particle, or by arrays that are bowl-shaped where the transducers all point towards a trap point [26]. To illustrate the shape of the acoustic field which is created by two arrays opposite to each other, the final array set-up from the array design chapter shown in Figure 4.4 is simulated below in Figure 3.7. It can be seen in this figure that the two arrays form a standing wave between each other that creates a line of alternating nodes and anti-nodes where multiple particles can be trapped together as shown physically in Figure 4.4. It is also clear that this field creates much larger pressures as the scale is twice as large as the single-sided arrays.

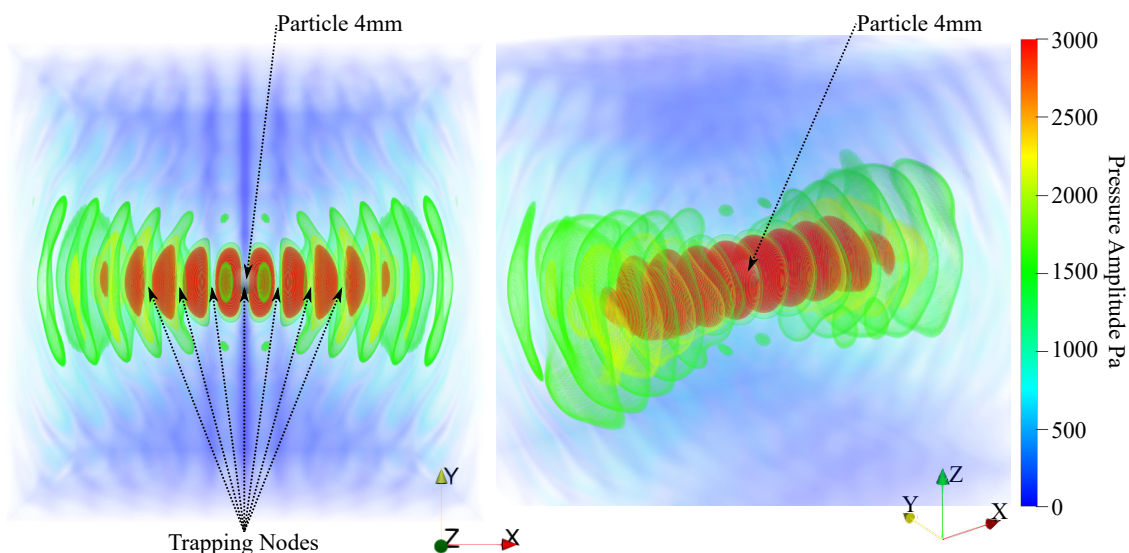


Figure 3.7: Two 3D plots, from the side on the left and isometrically on the right, showing the absolute value of the complex acoustic pressure for a twin trap with a plane between the two arrays. Calculated with the same array set-up shown in figure 4.4 with the two arrays 10 cm apart. The transducers are not visible in the calculated boundary.

Unlike the single-sided arrays which produce a single strong trap point with some other smaller trap points, the two-sided array creates multiple trap points in a line that can all trap particles at the same time. This is more easily illustrated if the acoustic potential field that these arrays produce is plotted. Shown in Figure 3.8 is the potential energy field that is produced by the pressure field shown in Figure 3.7. From this field, it can be seen that multiple trap locations are produced by this array set-up meaning that multiple particles can be trapped. The strengths of these minima are discussed in the trap characterisation section 5.2, but it can be seen from the potential energy graph that these minima are much lower than the minima shown in Figure 3.4. As the trapping forces

are stronger with these types of traps, it allows for the trapping of denser materials. It is therefore essential to be able to characterise these minima to discover what materials can be trapped by them.

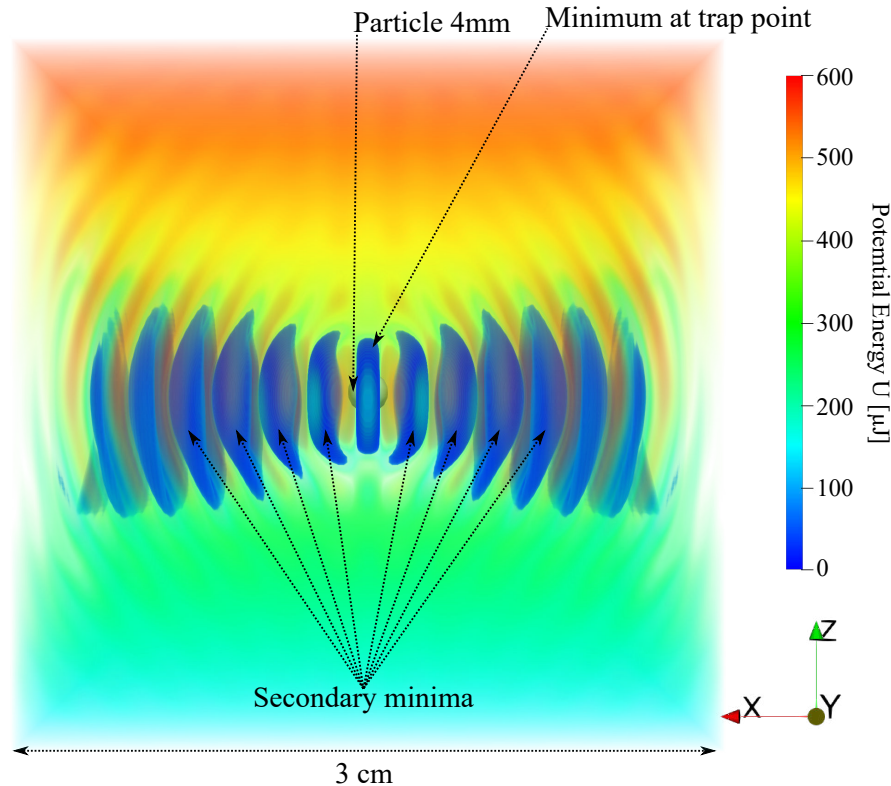


Figure 3.8: 3D plot showing the same field as in Figure 3.7 but displaying the acoustic potential  $U$  (including gravitational potential energy). The plot shows the shape of the acoustic potential field in 3D and clearly illustrates a minimum at the trap location, with multiple minima on either side.

For the investigation of these trap types in reality, a single-sided computer-controlled array of individually controllable transducers is built. A second identical array is built to investigate the effects that can be created with multiple acoustic arrays, including levitating denser materials and creating stronger traps. The choice of transducer size is arbitrary; the smaller the transducers are, the cheaper they become up to a point. If smaller transducers are used, arrays with more transducers can be constructed with the same budget. Small 1 cm transducers are chosen to fit these specifications as they are readily available and proven to work on previous projects [3]. The size of the particles that can be levitated by the acoustic traps is defined by the wavelength of the sound waves, as particles that are larger than half the wavelength interact with multiple waves at once and can become unstable in the trap locations. The selected transducers have an optimum frequency of around 40 kHz, therefore, they can levitate particles with a diameter smaller than 4 mm. This frequency is in the ultrasonic region which is inaudible to humans. The mass of the particles which can be levitated is defined by the power that can be outputted by the array; higher power will create larger trapping forces allowing denser particles to be held.

---

CHAPTER  
**FOUR**

---

## PHASED ARRAY DESIGN AND CONSTRUCTION

Ultrasonic transducers work in the same way as a typical speaker by vibrating a small plate back and forth at the frequency and amplitude defined by the input signals frequency and power, respectively. They also resonate at a specific frequency dependant on their construction which can vary by plus or minus 1 kHz. If the transducer is driven at a different frequency to its resonant frequency, then it will output less power than it otherwise could. To be able to control the phases of all the transducers, a signal needs to be sent to each transducer individually with a delay in time of a fraction of the frequency. The primary design constraint is the signal generation, as the array requires a 40 kHz phase shifted signal for each transducer, the more transducers that are added or, the finer the phase resolution, the faster the computers update speed needs to be.

The phase resolution is the fraction of  $2\pi$  that the controlling computer can offset one transducer compared to another. Since the frequency of the sound is 40 kHz, if you had two transducers one offset from the other by half a wavelength or  $2\pi/2 = \pi$ , the controller needs to be able to update the transducers at four times the original speed; 160 kHz =  $(40 \text{ kHz} \times 2 \times 2)$  as it now has to send signals to two transducers with one of them offset from the other by half a wavelength, this gives a phase resolution of  $\pi$ .

It is possible to run a 64 transducer board with either a Raspberry Pi or an Arduino Mega [4] with a phase resolution of  $2\pi/10$ . It is decided that controlling the board with one of these mini computers is not sufficient enough as the investigation of very high phase resolutions is desired and being able to control the phases of all the transducers precisely is a desirable trait for the array board to have.

To facilitate this need, it is decided to use an FPGA to control the transducer board(s). A field programmable gate array (FPGA) is a computer chip that has programmable hardware inside it. This means logic can be programmed into hardware and high-speed specific computations can be completed. This is used to create a very fast internal clock in the MHz range that allows the array board to be controlled with a phase resolution of  $2\pi/1250$  which is far beyond the required precision of previous designs [4].

Before the transducers can be used polarities are tested as the manufacturers positive and negative markings on the transducers are found to be randomly placed and do not correspond to the correct polarity. The polarity is important as if a transducer is connected in one direction then an initial positive input signal will result in an initial positive output

signal but if the transducer pins are reversed an initial positive input signal will result in an initial negative output. This is a problem as if they are not checked some of the transducers will be permanently offset from others by half a wave. The polarities are checked with an oscilloscope by moving the speaker diaphragm and watching the outputted signal, the correct pins are marked and can be used in the construction of the array.

To keep the costs reasonably low the board design had to fit on the standard PCB size of 10 cm × 10 cm. The board layout is designed and sent to an external company for manufacture. The transducers, amplifiers and capacitors are all soldered into place checking that the circuits have not been shorted after each new component is added. These PCB boards facilitate the whole array to be self-contained on one board. The FPGA chip is also located on the bottom of this board shown in Figure 4.1 which allows the board to be fully contained and only require external power and a serial data connection to a computer to feed instructions to the FPGA chip.

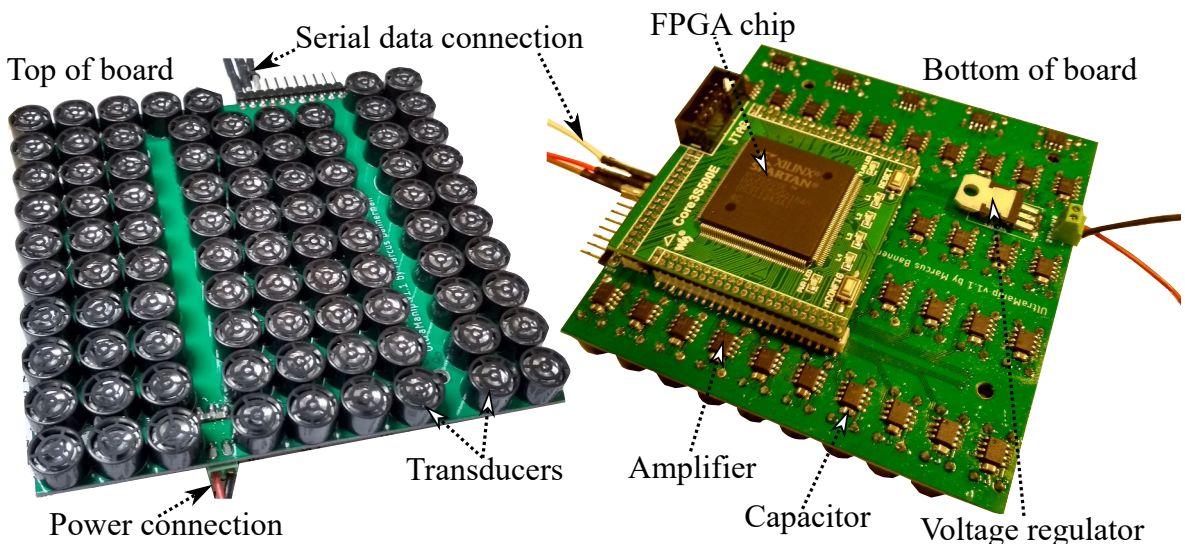


Figure 4.1: Two photos showing the first completed transducer array board and all of the components. 88 Transducers in a regular grid pattern on the front with the amplifiers and capacitors on the reverse, the FPGA chip is mounted on the back of the board.

For the flat array that is constructed, shown in Figure 4.1 there are 88 transducers connected to the FPGA chip through amplifiers which boost the power of the weak signals from the FPGA high enough to drive the transducers. The FPGA outputs square wave signals to the transducers as these allow for the maximum output power possible from the transducers. The transducers still output a sine wave as their physical construction is piston-like and cannot output a square wave.

For future experimentation and ease of use, it is decided to add Arduino mini computers to the board's serial inputs that in the future will allow the boards to be controlled wirelessly and not require a direct connection to the controlling PC. Initially, these computers are set up to pass through the serial signals from the controlling PC to the boards themselves.

A second board is built to the same specifications as the first, allowing for future

physical testing of stronger two-sided acoustic traps. To create these traps, precise relative placement of the arrays is required. Therefore it is decided that a frame to hold the arrays in place is required. Aluminium profiles are found to be a cost-effective means of building a custom frame to the required specifications; these profiles are customisable with any size and layout possible by nature of the modular construction of the different components. Shown in Figure 4.2 is the 3D modelled design of the frame, used to plan its construction and the final constructed frame. The frame allows modular movement of either array to any location inside or just outside of the frame. This allows for the whole system to be self-contained and does not require multiple parts to be operated.

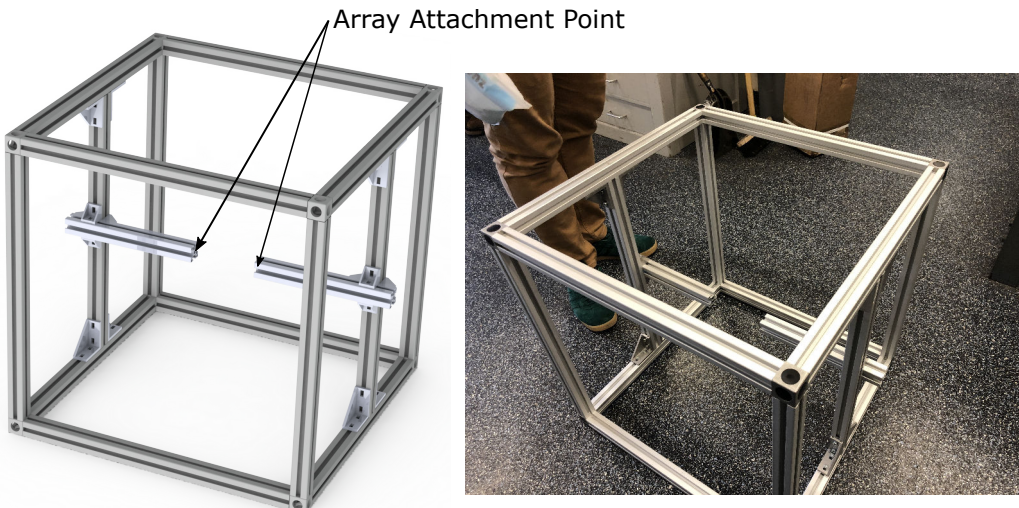


Figure 4.2: 3D model created in Solidworks of the proposed frame design on the left and the completed frame on the right.

To be able to attach the array boards to the frame a 3D printed mounting bracket is required, this is designed to be the inverse of the aluminium profile and therefore allows it to slide onto the frame and be easily removable. The design for this component is shown in Figure 4.3 where the mounting holes align with the pre-existing holes on the array board. The new system for sending commands to the board can be seen at the top of the array board on the right of the figure; this allows the array to be controlled with a micro USB cable and does not require a custom cable like the initial version. In the future different attachment methods could be used to be able to change the angle of the boards to whatever is required. Initially, they can only be at 90 degrees to each other as this is the most straightforward to implement.

Two mounting brackets are printed which allows for the testing of two-sided acoustic trapping shown in Figure 4.4. An initial demonstration of the two-sided acoustic trapping was conducted, but an unforeseen issue arose halting work on this part of the project. Previous multi-array designs, for example, Asier's work shown in Ref. [4] uses the same controller for both arrays unlike the of shown in Figure 4.4 that are both independent from each other. It is found that their internal clocks do not stay in sync and therefore when phase offsets are sent to each board they drift from each other this stops the acoustic traps from consistently forming. This problem is rectified by adding a syncing line between the

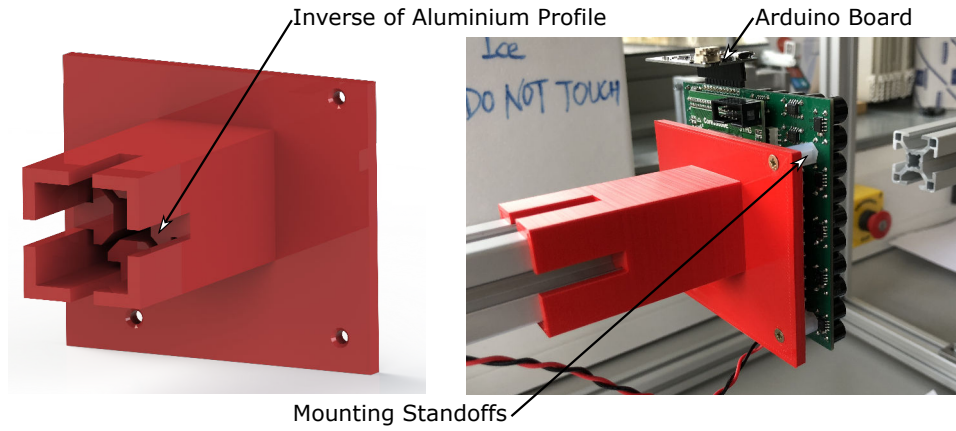


Figure 4.3: 3D model created in Solidworks of the proposed array board mounting bracket on the left and the completed assembled bracket on the right. The updated control system can be seen on the top of the completed board where the Arduino is connected directly to the array board.

boards that cause the arrays to reset their clocks at the same time and therefore keep their phase offsets correct relative to each other. This change is vital to be able to work on the physical two-sided trapping side of the project and as it is still inoperable, this is left to be continued in future work.

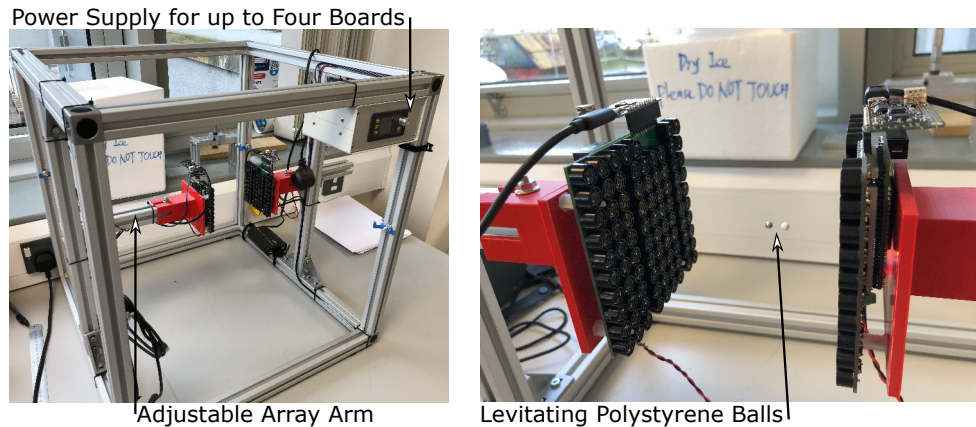


Figure 4.4: Picture of the final two-array set-up showing the fully self-contained unit which includes a power supply and control cables allowing the array to be programmed and controlled on the left, and the initial testing of two array acoustic trapping which has two polystyrene particles trapped in standing wave trap points on the right.

To demonstrate the arrays abilities, multiple operating modes are programmed to display the arrays different features. The most basic operating mode is focusing mode where the user can input a location in space relative to the array's axis shown in Figure 4.5 and the array will adjust the phases of the transducers so that all the sound signals arrive at the focus point in phase. This is achieved using a simple algorithm that calculates the separation vector from each transducer in turn to the focus point as:

$$\vec{r}_s^i = \vec{r} - \vec{r}_t^i$$

Then calculates the magnitudes of the vectors which gives the distances from the trans-

ducers to the focus point:

$$d(r^i) = |\vec{r}_s^i|$$

Finally calculating the phase shift/delay of each transducer as  $\Phi$ , where  $\lambda$ , is the wavelength of the sound wave and mod 1 takes the decimal part of the division result:

$$\Phi = (1 - ((d(r^i)/\lambda) \bmod 1)) \times 2\pi$$

As an example, if there are two transducers, one 4 cm away from the focus point and the other 5 cm away, with the wavelength as 3 cm. Ignoring the multiply by  $2\pi$  as that converts the fraction into radians. The 4 cm transducer has a shift  $\Phi = 0.666 \times \lambda$  which is 2 cm and the 5 cm transducer has a shift  $\Phi = 0.333 \times \lambda$  which is 1 cm. Therefore with these shifts, both transducers are now equivalently 6 cm away from the focus point.

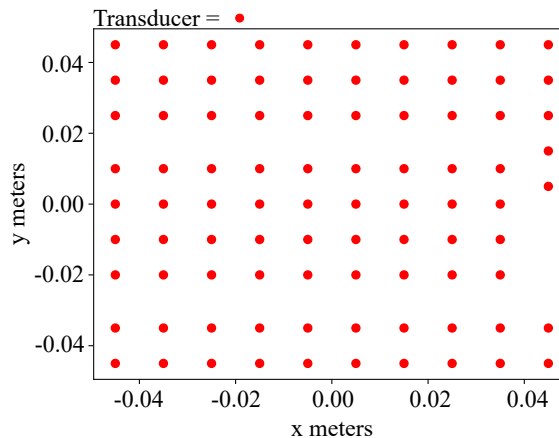


Figure 4.5: Array grid reference axis where focus points are relative to this axis, the z-axis is positive in the upwards direction from the array.

The primary trapping mode uses the holographic acoustic elements described in Figure 3.2 that can be selected as either Twin, Vortex or Bottle. The bottle trap has only been proven in theory to be able to trap particles and has yet to be demonstrated physically. This mode works in the same way as the focusing mode with the addition of the holographic acoustic element onto the focused array pattern to form the acoustic traps at the desired locations. This mode has a fixed trap location where the particle can be manually moved into the trap with tweezers or lifted with acoustically transparent mesh.

Another mode implemented to demonstrate particle movement takes in an initial location and a movement pattern, for example, a ring at a certain height. The algorithm then uses the trapping mode with a predefined trap type and holds a trap in place for a certain amount of time to allow the particle to be placed in the trap. The trap location is then updated in small increments around the movement pattern allowing the particle to be moved in circles. This mode requires more work, as when the algorithm starts up the particle is at rest and is then accelerated very quickly, this can cause the particle to be thrown out of the trap. To mitigate this, the mode will need to slowly ramp up and down when it moves

---

so that the particle has time to change its velocity without becoming unstable. It may also be possible with particle tracking to estimate where the particle will be in the future which will allow for the trap to be slightly ahead of the particle and therefore permit faster changes in direction as the inertia of the particle is dissipated by the more accurate trap positioning.

Another application of phased acoustic arrays is Haptic Feedback, a basic version of this is implemented as a Haptic Feedback mode. This is achieved using the focusing mode and focusing the array at a location in space and then modulating the power of the array at a much lower frequency than the transducers run at. Modulating, or turning the array on and off, at 200 Hz gives the strongest feeling to receptors in the human skin [10]. This creates a region in the air at the focus point that becomes an audible sound source to humans due to the sound from ultrasound effect [12]. This point can be felt on the skin and is similar to feeling a light fuzzy object. It can also be used in parallel with the movement mode and therefore can be moved around in patterns to create specific sensations. This technology is being used in conjunction with virtual reality devices to allow for sensations to be created in the air that mimic the virtual environment [11].

Using this same effect but instead of modulating the array at a single frequency, modulate it with an audible sound source like an audio file or speech. The focus point in space can be used as a sound source that appears in mid-air while the array is still silent to humans. This could be used directionally or towards specific individuals or groups of people in a room allowing them to hear audio that no one else can. This mode is yet to be implemented on the array but is possible with further work in the future.

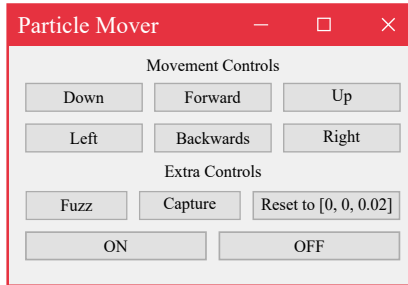


Figure 4.6: Vector version of the GUI that can be used to move particles in 3D space. The controls are linked with the acoustic algorithms and are able to calculate and move the particle in real time. It can also be used to turn the array on and off easily.

A GUI (Graphical user interface) is programmed to allow for a user-friendly way of controlling the acoustic trapping software, shown in Figure 4.6. A predefined trap type is used and the trap can be moved through space with the button controls. The focus point can also be reset to a predetermined location and the array toggled on and off. The capture mode is programmed to raise the trap slowly and can be used to lift particles off a mesh netting that is suspended above the array.

---

CHAPTER  
**FIVE**

---

## SIMULATION OF ACOUSTIC FIELDS

### 5.1 Acoustic Model Calibration

Calibrating the computer model to the physical array is necessary to be able to calculate forces and acoustic potentials that are present, making the model predictive of the physical array. This calibration requires the constants of the acoustic pressure equation Eq. 2.3.1 and the Gor'kov potential Eq. 3.2.1 to be determined. To test that the array is producing sound at 40 kHz an oscilloscope is connected across the pins of a transducer which is then held above each transducer in the array. The oscilloscope displays the frequency of the sound that the transducer is outputting, confirming that the array is outputting sound at the desired frequency. The output power of each of these transducers will vary based on the resonance of the array transducers and the measuring transducer, each transducer has a specific resonant frequency which when driven at, will produce its highest possible output power and at other frequencies gives a worse output efficiency.

The particle and the medium densities are required for the Gor'kov potential equation. Assuming that air is an ideal gas the density of air at sea level and at 20°C is given by  $\rho = N m/V = p m/(R T)$  with the molar mass of air as 29 g/mol, therefore the density of air  $\rho = 1.20 \text{ kg/m}^3$ .

The density of the particles which in this case are polystyrene balls are also required. This is achieved using a pan balance and weighing a select number of spheres of known size and using the mass and the volume to calculate their densities.

Table 5.1: Diameters and volumes of polystyrene particles for density calculation

Particle	Diameter (mm)	Volume ( $\text{m}^3$ )
1	5.57	9.04824E-8
2	5.93	1.11409E-7
3	5.58	1.1074E-7
4	5.14	7.1103E-8
Totals		3.84E-7

Shown in Table 5.1 is the total volume of four polystyrene particles, this was calculated with their diameters, measured with electronic callipers, assuming they are perfect spheres. This is an approximation as the spheres are soft and therefore not perfectly spherical, although it is still valid as a guide to the actual density. The mass from the pan balance for the four particles is 0.0066 g this is the apparent mass of the particles as it is not taking into account buoyancy forces. The actual mass is given by:  $\text{mass} = \text{mass}_{\text{apparent}} + \rho_{\text{air}} V_{\text{particles}} = 6.6 \times 10^{-6} \text{ kg} + 1.20 \times 3.84 \times 10^{-7} = 7.1 \times 10^{-6} \text{ kg}$ .

This leads to the density of the polystyrene spheres being the total mass divided by the total volume of the particles.  $\rho_{\text{particles}} = 7.1 \times 10^{-6} \text{ kg} / 3.84 \times 10^{-7} \text{ m}^3 = 18.5 \text{ kg/m}^3$ . Comparing this density to literary sources where the density of expanded polystyrene ranges from 11 to 32 kg/m<sup>3</sup> [27] the calculated density is acceptable.

The amplitude constant which defines the power transferred by the transducers is an efficiency and is dependent on the specific transducers that are used, the array layout and its construction. To calibrate this number, a particle is levitated at a known height and the voltage of the array is then lowered until the particle is dropped. This then allows the model to be set at that voltage and the amplitude constant adjusted until the simulated potential energy shows an inflection point at the trap location. This inflection point demonstrates that a particle would be dropped as the vertical forces on the particle would sum to zero. Once the amplitude constant is found, the voltage can be set at any arbitrary value the array can match and the model will be able to predict if levitation at that point is possible accurately.

Levitating a 4.2 mm polystyrene particle at 1.8 cm above the centre of the acoustic array and then lowering the voltage until the particle was dropped allows a dropping voltage to be found. This process is repeated multiple times to get an average voltage. The voltages recorded are shown in table 5.2 this gives an average voltage of 12.30 volts to be used in the simulation.

Table 5.2: Voltage of the array when the particle is dropped

Attempt	1	2	3	4	5	Average
Voltage When Dropped	12.10	12.18	12.17	12.45	12.58	12.30

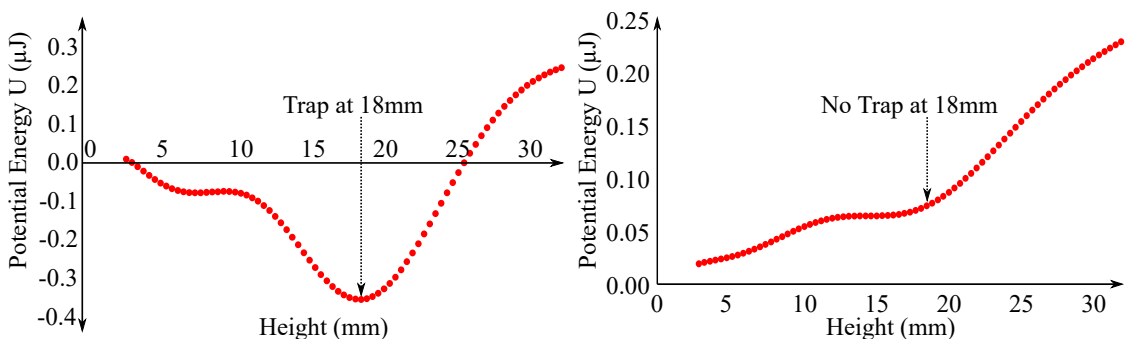


Figure 5.1: Graphs of potential energy at different heights above the acoustic array, on the left with an amplitude constant of 1 and on the right with the calibrated constant of 0.364.

Setting the amplitude constant to 1 when all the other constants are set shows a minimum in the potential energy in the z, or upward direction. This minimum in the potential energy is shown on the left of Figure 5.1 meaning that the particle is predicted to not fall down at this voltage which is incorrect compared to the physical array. The amplitude constant is iterated downwards until the potential energy shows an inflection point at the trap location meaning it would just support the particle and no more meaning, in reality, it would drop. Using an algorithm that checks if the next point is higher or lower than the previous the inflection point can be found. Shown on the right of Figure 5.1 with an amplitude constant of 0.364 it is shown that the particle would be dropped by the array. The voltage can then be set back to its maximum value of 18 volts to show that in the simulation the particle would be levitated, confirming what is seen with the physical array.

It has been demonstrated that dry ice can be used to image the acrostic pressure field, as the cold carbon dioxide creates a water vapour mist that is drawn to the high-pressure regions. A twin trap is set up and a particle levitated at 2 cm above the array. Images are taken while dry ice is held over the array allowing the mist to accumulate around the high-pressure regions. These images are compiled into a single composite image to allow the full trap structure to become visible. This structure is shown in Figure 5.2. It can be seen from the image that the acoustic field shape confirms the predicted shapes from the simulation of the twin trap shown in Figure 3.3. This confirmation further validates the model used to simulate the acoustic fields, although the model does ignore reflections and non-linear effects it is clear that these have little impact on the array if it is in an open environment. When two boards are close to each other, it may become important to include reflections in the simulations to accurately predict the generated acoustic fields.

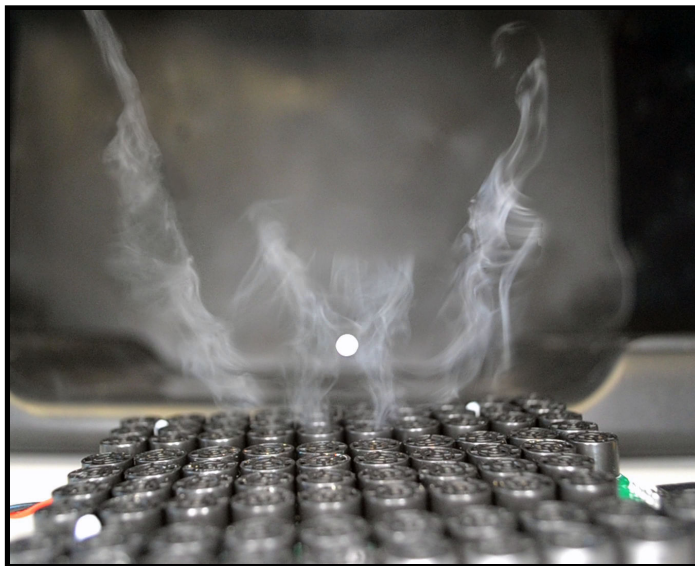


Figure 5.2: Composite image of five photographs of mist created by dry ice used to visualise the shapes of the acoustic field. A twin trap is used and a comparison can be made between the physical array and the simulated field shown in Figure 3.3. A 4 mm polystyrene bead levitating 2 cm above the array is shown in the centre of the image.

## 5.2 Acoustic Trap Characterisation

The ability to characterise different acoustic traps or the same trap at different locations is essential to be able to compare them quantitatively. Trap strength is one of the metrics that can be used to compare the different trap locations and is defined as energy difference between the bottom of the trap and the lowest edge of the trap, therefore, the minimum kinetic energy a particle would need to escape the trap. In the case of acoustic traps which are four-dimensional with three spatial dimensions and an energy dimension, the particle can be in a saddle point in any of the spatial dimensions. The trap is a minimum in all three directions giving it a volume where the particle will fall inwards if it is inside or fall away if it is outside.

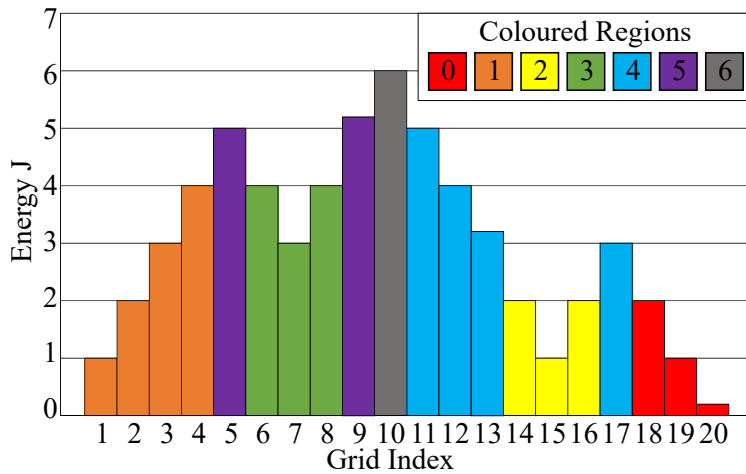


Figure 5.3: Test data for the trap finding algorithm, showing the expected region allocations in different colours for each of the grid voxels.

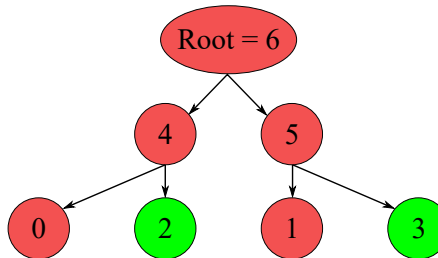


Figure 5.4: Region hierarchy output of the trap characterisation algorithm for the data shown in Figure 5.3, with regions connected to the outside marked in red and internal regions marked in green. The green nodes correspond to internal minima that can be clearly seen in Figure 5.3.

To be able to calculate the trapping escape energy, an algorithm to find trap regions in the potential energy matrix and characterise them is required. The goal of the algorithm is to categorise all points in a discrete grid of space as either outside or inside a trap and distinguish traps from each other. The way this is done is by starting with a sorted list of voxel locations by energy and checking all neighbouring cells then assigning it to a region based on how many assigned neighbours it has. The algorithm keeps track of this region

and can display it as a trap volume, this is discussed below. Working through the sorted list of locations from lowest energy to highest means by definition that any unassigned neighbour has a larger energy than the current voxel. The hierarchical algorithm is shown below in pseudo-code to illustrate how it is implemented in python.

1. Current region = 0
2. Select the unallocated voxel with the lowest energy in the grid. If there are no more unallocated points, halt
3. Collect all allocated neighbouring points of this voxel
  - (a) if none, allocate this point to region, add one to region counter
  - (b) if one, allocate this point to region of oldest parent of the neighbouring point or to the region of the neighbouring point if the neighbouring point has no parents
  - (c) else, check if multiple neighbours are in unique regions
    - i. if yes, allocate this point to region, set all neighbouring point's region's parents to region, add one to region counter
    - ii. if no, allocate this point to region of oldest parent of the neighbouring point or to the region of the neighbouring point if the neighbouring point has no parents
4. Return to step 2

Once the algorithm has completed, and all regions have been found any regions that are connected to the outside of the grid need to be discarded. This is done as any region that is connected to the outside cannot be interpreted as a minimum as it is not fully visible. To illustrate how this algorithm works and check that the algorithm is performing as expected, multiple simple test cases are built. A one-dimensional example set of data is shown in Figure 5.3. From this example, it can be seen that the lowest energy voxel, at index 20 is selected first and assigned region 0. The algorithm above is then followed through and all voxels assigned. The algorithm outputs a hierarchical tree structure shown in Figure 5.4 which displays which regions are connected to the outside and which regions are internal. There can be multiple internal regions connected to each other which is either due to small valleys connecting together like a rough surface at the bottom of a valley or from a few larger minima that share a border where neither of them are connected to the outside.

Distinguishing between these two cases is not an insignificant task. One method is classifying based on region volume, or how many voxels make them up; this can be a useful metric for determining if regions need to be merged or they are separate minima which share a border.

The algorithm assumes that none of the voxel's energy values are the same, this assumption is valid as the program stores the energy of each voxel as a floating point number so any two voxels having exactly the same value is not likely. Allowing the algorithm to work in higher dimensions introduced complications that needed to be overcome for the function to work. When there is only one spatial dimension like the data shown in Figure 5.3 each voxel either has one or two neighbouring voxels so a region cannot be neighbours to multiple voxels in the same region. A bug was noticed when testing the algorithm with two spatial dimension test data where a voxel can have four neighbours and circular regions can be formed. This allows for regions to be assigned to their own parents which is impossible and causes the algorithm to get stuck in an infinite loop. This is solved with step 3-C shown in the algorithm above where not just multiple neighbouring voxels are required, but multiple unique neighbouring voxels are needed to assign a voxel to a new region.

The algorithm can output various quantitative information about the field, that otherwise would be hard to determine from the complex 3D arrays of data like the ones shown in Figure 3.8 as a volume render. The algorithm keeps track of all regions and can output whether or not a specific region is connected to the outside of the boundary or is internal. It can also display the escape energy of any region, which is the difference in energy between the minimum of the region and its lowest edge. It can output the volume of the region which can be calculated from the number of voxels that the region has and the grid size that the field has been calculated on. Finally, it can display the location of the region's minimum, in space, this is useful in keeping track of where the trap has formed, compared to where the focus point is specified.

The three holographic trap types and their respective trap volumes and shapes are shown in Figures 5.5, 5.6 and 5.7 these volumes are created by the flat array shown in Figure 5.2. The front and side views of these figures show the output of the algorithm displaying the largest trap's voxels. The lowest edge potential energy value of the trap is taken for that region and used to create an isopotential surface contour shown isometrically on the right of all three figures. The bottle trap is calculated at a higher height as it does not form at the lower heights.

Using the hierarchical algorithm on a field that is multiplied by -1 means that minima become maxima and maxima become minima. In the same way that it can search for minima in the field, it is, therefore, possible for the algorithm to search for peaks in potential energy, which are areas where particles are repelled from. These locations are undesirable for trapping as they interfere with the arrays ability to trap particles consistently. These high energy regions may be useful in particle manipulation if the goal is to deflect particles rather than trap them.

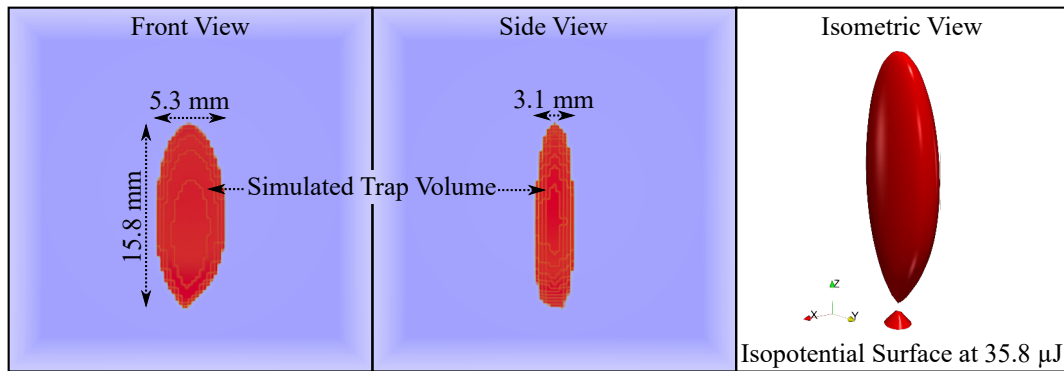


Figure 5.5: 3D volume representation of the twin trap simulated at 18 mm above the array with a 4.2 mm particle at 18 vptp. Inside the red volume, a particle will fall towards the centre of the trap, outside the red volume a particle will be pushed away from the trap.

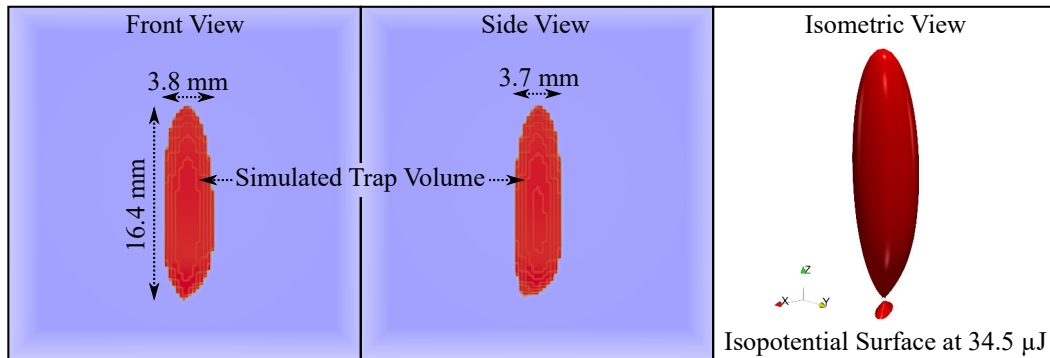


Figure 5.6: 3D volume representation of the vortex trap simulated at 18 mm above the array with a 4.2 mm particle at 18 vptp. Inside the red volume, a particle will fall towards the centre of the trap, outside the red volume a particle will be pushed away from the trap.

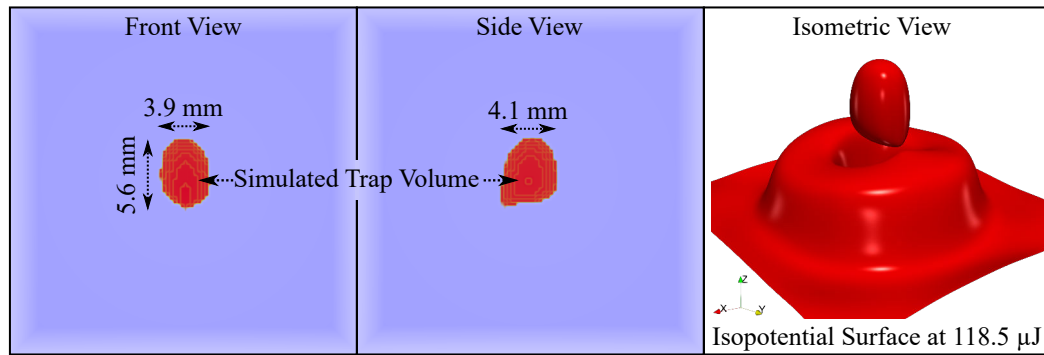


Figure 5.7: 3D volume representation of the bottle trap simulated at 24 mm above the array with a 4.2 mm particle at 18 vptp. Inside the red volume, a particle will fall towards the centre of the trap, outside the red volume a particle will be pushed away from the trap.

## 5.3 Acoustic Array Optimisation

Understanding the capabilities of the acoustic levitation array shown in Figure 5.2 is vital, it is desired to know the trap strength as a function of height over the array and the volume above the array it can trap particles. This is investigated by calculating traps at varying heights and allowing the algorithm to search for trap locations after each field has been determined. It is noticed that while calculating these fields, the results of the algorithm had discontinuities at 5 and 1 cm above the array. The potential energy at trap location is expected to fall off gradually and not as a step change discontinuation as is found in the data. Investigating this further revealed that since the algorithm is calculating the acoustic traps at specific locations, it would search for minima in a predefined grid around this expected location. Since the holographic method of applying a phase pattern to the focusing point pattern is not an exact method of calculating a minimum at a specific location, it is found that for the array layout that is built specifying a trap location anywhere above 5 cm, results in the height of the trap's minimum staying at 5 cm and not rising any higher. To solve the calculation problem of the trap energies, it is therefore required to make sure the calculation grid box is sufficiently large and in the correct location to capture the entire trap volume, or the algorithm will display that there are no minima.

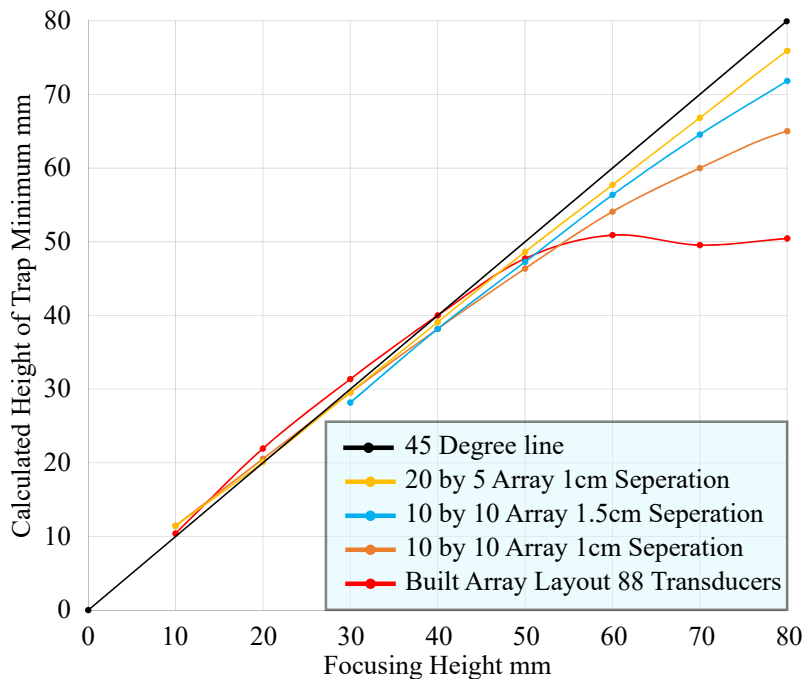


Figure 5.8: Graph displaying the variation in the calculated trap minimum height as a function of the focusing height. The grid layouts used are square grid patterns, except the built array which uses the layout shown in Figure 4.5. It is expected that the other lines would level off at higher heights but the trapping energy trends to zero above 8 cm for these arrays at 18 volts.

Plotting the calculated trap heights as a function of the focusing height for four flat array layouts is shown in Figure 5.8 where it can be seen for the built array that even if

the trap is focused above 5 cm the location of the trap stays around 5 cm, the trapping energy decreases, eventually to zero, as the focusing height is raised even though the trap doesn't move. This finding is corroborated by the physical array where the particle cannot be levitated above 5 cm, and when the trap is slowly raised higher, the particle vibrates around 5 cm until finally being dropped. This height limit is partly due to the aspect ratio between the particle location and the shape of the array, where if the particle moves further away from the flat array the angle between the transducers and the particle tends to 90 degrees. At this point, the waves from the transducers are no longer partially coming from the side of the particle but all from below where they cannot form an acoustic trap.

In Figure 5.8 it can be seen that from the red line to the orange line, adding more transducers to the same area causes the calculated minima to more closely match the focusing height and that a regular grid also allows for a closer match at lower heights. Spreading the same number of transducers out in a larger square pattern shown from the orange to blue line, where the orange array is 10 cm by 10 cm and the blue array is 15 cm by 15 cm, each with 100 transducers, it can be seen that a larger footprint allows for closer matching at higher heights. This method is not ideal as can be seen that this array cannot form traps below 3 cm. The final method is to arrange the same number of transducers in a rectangular 20 cm by 5 cm arrangement which allows for the best matching at the low and high focusing heights. Not shown is that increasing the voltages of these arrays causes the lines to move closer towards the 45-degree line, therefore increasing power to the arrays causes more reliability in trapping locations.

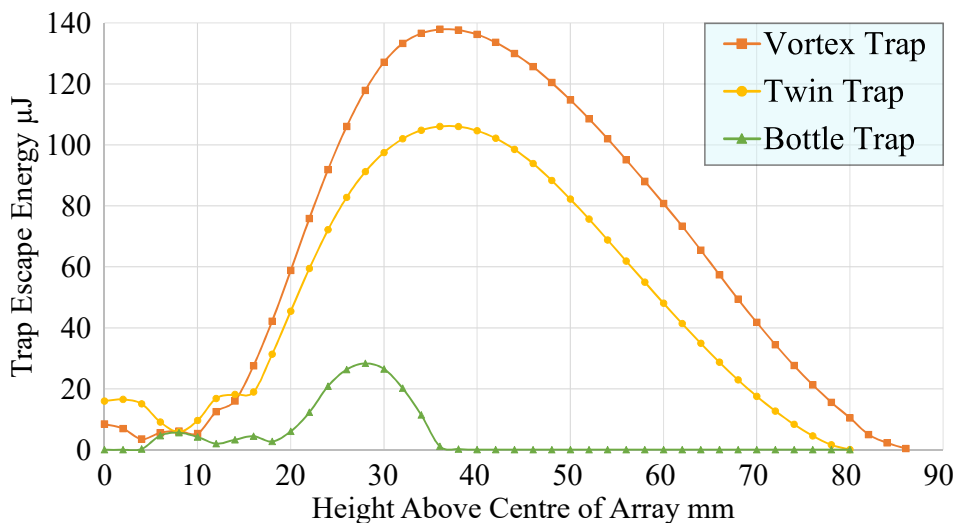


Figure 5.9: Graph showing the change in trap strength as a function of height above the centre of the built array for the three holographic acoustic trap types.

It is useful to know the trap strength as a function of height above the array as this allows for the location of the maximum trap strength to be found. Shown in Figure 5.9 is the trap strength in  $\mu\text{J}$  plotted against the focusing height above the centre of the built array with its layout shown in Figure 4.5. This is calculated using the trap finding algorithm which searches for the trap in the acoustic potential field that is simulated for every height

and for all three holographic trap types. It can be seen from the graph that above 15 mm the vortex trap produces the strongest traps for all heights followed by the twin trap at around 30% weaker at the maximum value. The maximum trap strength is achieved at 36 mm for both the vortex and the twin trap types and the maximum for the bottle trap is at 28 mm, this corresponds directly with its circular signature shown in Figure 3.2 set at a diameter of 30 mm. For the bottle trap this signature diameter can be adjusted to best match trap strength at a specific height, but on arrays with a limited number of transducers, it is difficult to form this trap type as shown on the graph where at most heights, the bottle trap does not form. It is also notable that the point on the graph where all three trap types have the same trap escape energy is the height equal to one wavelength of the transmitted sound  $\approx 8.6$  mm.

Taking the height as the height of maximum trap strength equal to 3.6 cm above the array, it is investigated over what area above the array acoustic traps can form and the comparison of their strengths to each other. It can be seen from Figure 5.10 that both arrays produce a circular mostly symmetrical pattern of trap strengths over their centres. On the right, the built array produces around 34% less maximum trapping strength compared to the 10 by 10 square grid pattern array on the left. This difference is mainly due to the different number of transducers 88 compared to 100, this decrease in total number of transducers is small at 12% although it results in around 34% less maximum trapping strength. The other factors impacting the difference in trapping strength include the asymmetrical layout of the built array and the interference patterns that introduces.

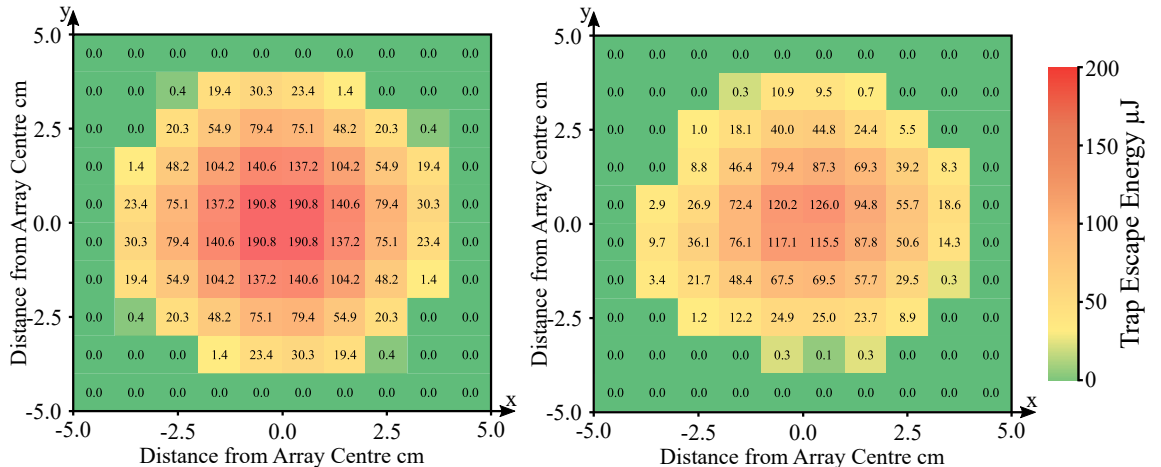


Figure 5.10: Heat maps displaying trap strength as a function of x-y position above two arrays using a vortex trap at the maximum trap strength height of 3.6 cm above the centre of the arrays. Left with a 10 by 10 square grid array and right with the built array layout shown in Figure 4.5. Zero trap energy corresponds to no trap formation.

The placement of the transducers is vital in determining what shapes of acoustic fields can be produced. It is possible to arrange the shape of transducers so that they create trapping fields by being spatially separated in a specific way, so they do not have to be individually controllable to create acoustic traps. This is useful for low budget demonstrations and proof of concept since these arrays are not controllable and have fixed trap

sizes and locations. A design that makes use of this concept is shown in the Instructables project of Ref. [28]. It is also possible to have a fixed transducer and a shaped reflector that is able to form specific acoustic trap points [29].

Shown back in Figure 3.3 other regions of high amplitude pressure are visible that are not desired, these secondary maxima are unwanted and may be caused by the regular array patterns. This problem is directly related to beamforming microphone arrays which are designed to pinpoint the source of sound waves or to improve the sound to noise ratio of microphone arrays [30]. Using the addition of noise or specific array layouts it may be possible to eliminate these secondary maxima.

The other side of this problem is trapping strength, creating the maximum trapping strength possible requires the maximum number of transducers in the smallest area. To fit the maximum number of transducers into the smallest area in two dimensions for circles is to use a hexagonal packing pattern [31]. This pattern is a regular packing and has the same secondary maxima issues that are shown in the square packing example in Figure 3.3. To investigate this effect, shown in Figure 5.11 is the acoustic trap escape energy plotted against the packing efficiency of multiple arrays for the vortex and the twin trap types. Packing efficiency is the area taken up by the transducers divided by the area of the smallest box that constrains all the transducers. The highest efficiency is the hexagonal packing which has an efficiency of  $\approx 90.6\%$ ; the other packing efficiencies are created by spreading the same number of transducers out over a larger area in the same layout. It can be seen from Figure 5.11 that there is a linear relationship between the packing efficiency of the transducers and the trapping strength. This holds true for both the vortex and the twin trap types.

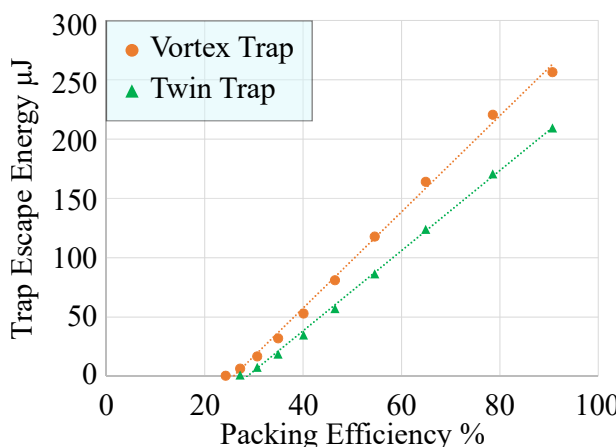


Figure 5.11: Trap strength as a function of transducer packing efficiency where a 10 by 10 square grid array is used and the trap is calculated at 3.6 cm above the array's centre.

It is expected that there would be a linear relationship between the transducers power and the calculated acoustic trap strength. As can be seen from Figure 5.12 the energy required to escape the acoustic trap is not linear but actually related to the square of the array power by the relationship:

$$E_{Escape} = 1.103 V^2 - 2.578 V - 55.142$$

Where  $E_{Escape}$  is the energy required to escape the acoustic trap in  $\mu\text{J}$  and  $V$  is the acoustic array voltage in volts. For a vortex trap at 3.6 cm above the centre of a 10 by 10 hexagonal grid array. This result shows that an increase in voltage from 10 to 11 volts only adds  $\approx 20 \mu\text{J}$  to the trap strength compared to a voltage increase from 25 to 26 volts adding  $\approx 54 \mu\text{J}$ . It is unknown what causes this relationship, it may be due to the acoustic trap forming more completely at higher voltages with less interference, although this does not explain the non-linear trend of the escape energy compared to array voltage. Further investigation of this phenomenon is therefore required.

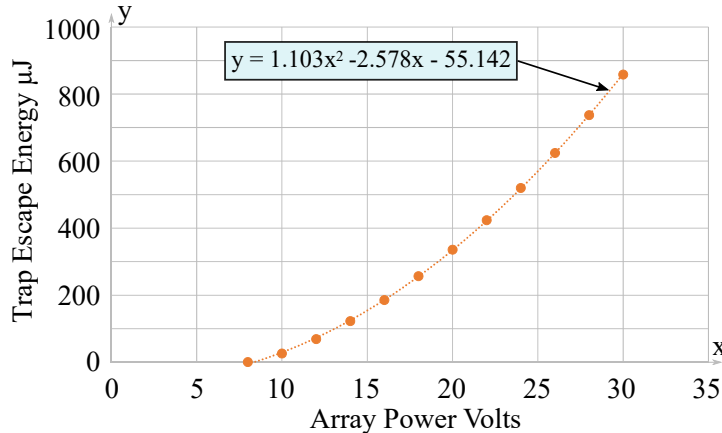


Figure 5.12: Trap strength as a function of array power where a 10 by 10 hexagonal grid array is used and the vortex trap is calculated at 3.6 cm above the array's centre.

The physical acoustic array cannot offset the phases of each transducer with infinite precision as the simulation can. So far the simulations have been run with a phase resolution of  $2\pi/1250$  as this is the resolution possible with the built array using the FPGA. It has been shown that acoustic trapping is possible with a phase resolution of  $2\pi/10$  by Asier Marzo [3]. To mimic the phase resolution in the simulations the output of the phase offsets, which are floating point numbers, are discretised into a set number of phases between 0 and  $2\pi$ . Therefore with a phase resolution of 2, each transducer offset would either be rounded to 0 or  $\pi$  depending on how close they are to either. The phase resolutions impact on the acoustic trap strength is plotted in Figure 5.13 where it can be seen that higher phase resolution has little impact on trap escape energy after 20 discretisations. It is clear from this data that the built array's phase resolution of  $2\pi/1250$  is excessive and not necessary to achieve the same trapping results. Not shown on the graph is that the trend continues to infinity where the maximum trapping strength remains constant for any phase resolution above 20.

These simulations can give insight into what an optimal single-sided array should be to achieve maximum possible trapping strength. It is clear that higher array voltage gives stronger trapping forces so the highest power possible to the array will give the strongest acoustic traps. The phase resolution of the optimised array would only need to

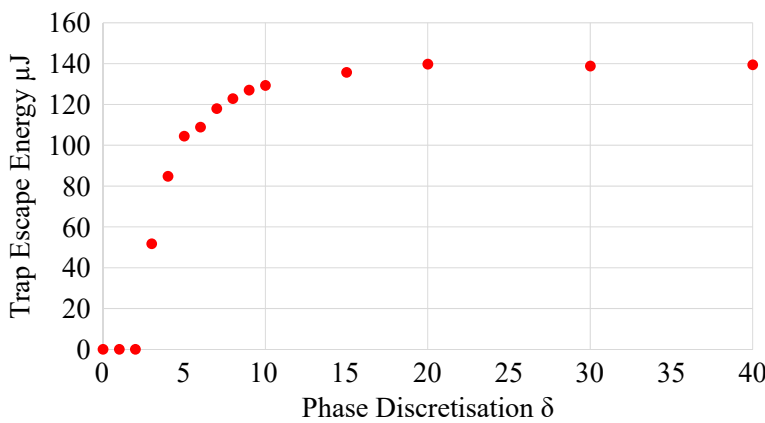


Figure 5.13: Trap strength as a function of phase discretisation where the built array is used and the vortex trap is calculated at 3.6 cm above the array's centre. Phase discretisation is the number of values as a fraction of  $2\pi$  the transducers phases can be set at.

be in the order of  $2\pi/20$  to achieve the maximum possible trapping strength. The packing efficiency relationship proves that packing the most transducers into the smallest area gives the strongest traps and therefore hexagonal closed circle packing should be used to achieve the strongest trapping energies. The positioning of the trap above the array is vital in achieving the strongest traps. Depending on the requirements if certainty in height above the array is desired, then the more spread out the footprint of the array the closer the match between the focusing height and the actual trap height. Otherwise, if the strongest trap is desired, then there is an optimum height above the array depending on its size where the trapping strength is maximum. Having the trap in the centre of the array will also give the strongest possible traps. There are many other factors that can influence the performance of the arrays, for example, acoustic reflections; if the array is in close proximity to surfaces that can reflect sound, then the reflections will cause interference and stop the traps from forming. The diameter of the levitated particle is also a significant factor on the performance of the array, if it is too large no traps will be formed. The densities of both the medium and the particle are major factors in determining if the acoustic traps will be able to hold the particle, these can be adjusted in the simulation and the trap finding algorithm is able to determine if a trap has formed or not around that particle. This is tested by changing the density of the particle to  $1000 \text{ kg/m}^3$  which is around the density of water and it is found that the single-sided array produces no traps at any height with a particle so dense. However, if the array layout shown back in Figure 4.4 is simulated, it is found that with this array layout and both boards perpendicularly separated by 10 cm, it is possible to trap particles with a density of up to  $3150 \text{ kg/m}^3$ . Therefore this array layout could easily trap water and could even trap a small sphere of aluminium and is very close to being able to trap diamond. This is compared to the single-sided array which when simulated can only levitate particles up to  $70 \text{ kg/m}^3$  which is almost two orders of magnitude less. If it could be kept cold enough, the single-sided array would be able to levitate liquid hydrogen. Therefore transducers orientation compared to each other is vital in creating the strongest possible traps.

## 5.4 Particle Simulation

Using the acoustic potential model for the generation of the acoustic fields described in the previous sections, it is possible to model particle moments in the acoustic field using basic particle simulation software. This is implemented in python to be able to map the paths of particles due to the forces caused by the acoustic potential field Eq. 3.1.1. Using these results to test whether or not a particle will be held in a trap or not and how it will move in space due to the acoustic radiation forces. The other benefit of modelling particle movements in space is that it allows for inertia to be taken into account, where if a particle is already moving it will require deceleration before it can be trapped. In future, this type of modelling would be able to be used in deflection and sorting mechanism testing.

A basic forward Euler method is first implemented where the particle will have three parameters namely position  $\vec{r}_i = [x, y, z]$ , velocity  $\vec{v}_i = [v_x, v_y, v_z]$  and mass  $m$ . A time step  $\Delta t$  and a force on the particle at all points in space will need to be calculated. The force of gravity will be included as  $F = mg$  with  $g$  as the acceleration due to gravity on earth as  $9.81 \text{ m/s}^2$ . With  $j$  representing the time step, the next position of the particle can be calculated as:

$$\vec{r}_i^{j+1} = \vec{r}_i^j + \Delta t \vec{v}_i^j$$

The new velocity of the particle can be calculated as:

$$\vec{v}_i^{j+1} = \vec{v}_i^j + \Delta t \frac{\vec{F}^j}{m_i}$$

This process of calculating the new position and the new velocity at every time step is a rudimentary way of particle simulation. This process neglects any resistances from air or other particles or solid boundaries. Ignoring these resistances for a single particle in an acoustic potential field and with gravity acting on the particle, it will still give a reasonably accurate simulation of how the particle will move. The issue that arises when using the forward Euler method described above for an oscillating system, like the particle in an acoustic trap, is that the numerical integration method adds energy over time and therefore will resonate back and forth until it has enough energy to escape the trap. This is not an accurate description of reality where the particle can be held indefinitely as long as the array is powered.

This can be overcome by using another method to integrate the equations of motion, namely the Verlet Algorithm which is third order for position and second order for velocity. The method is a central difference method compared to the forward Euler method which as the name implies is a forward calculating method. This method is generally used in molecular dynamics simulations as it is more accurate as it is higher order and does not require significant extra computations compared to the forward Euler method [32].

Similarly to the forward Euler method, the position at the next time step can be calculated as:

$$\vec{r}_i^{j+1} = \vec{r}_i^j + \Delta t \vec{v}_i^j + \frac{\vec{F}_i^j}{m_i} \frac{\Delta t^2}{2}$$

The new velocity of the particle can then calculated as:

$$\vec{v}_i^{j+1} = \vec{v}_i^j + \frac{\Delta t}{2} \left( \frac{\vec{F}_i^j}{m_i} + \frac{\vec{F}_i^{j+1}}{m_i} \right)$$

Using this method and a sufficiently small  $\Delta t$ , it is possible for the method to be used in oscillatory systems without adding energy and causing them to become unstable. Using this method, it is possible to set a particle in motion in a set acoustic field and then update that field whilst the particle is in motion. This could be used to create automatic systems for particle sorting and testing of different array layouts without having to construct physical arrays.

Currently, these methods are implemented in python and are not optimised for speed meaning that to have a sufficiently small  $\Delta t$  the algorithms take hours to run. These methods and the acoustic field calculations need to be implemented in c or another low-level programming language where there is significantly less computational overhead to make the simulations possible for enough time for results to be found. Other methods for speeding up these simulations is to use pre-calculated fields in the simulation and interpolate at each point in space, this would save time whilst running the simulation, although this method does introduce errors in the force and potential calculations as a predefined grid of points is used instead of calculating each point when required. This is a promising future research opportunity to build on the acoustic model and simulate particle moments in the fields.

---

CHAPTER  
**SIX**

---

## CONCLUSIONS AND FUTURE WORK

Single-sided and controllable acoustic levitation are both very new fields where many different applications have yet to be considered. This thesis investigates the basic background theory of sound and where the acoustic radiation force originates from, it explores the simulation of the acoustic fields with arbitrary array layouts and initial transducer phase inputs. An algorithm is developed and uniquely applied to search for acoustic traps in simulated acoustic fields. The ability to characterise the acoustic traps has led to the investigation of many different factors contributing to the strength of the calculated acoustic traps. The acoustic model is calibrated to the physical flat ultrasonic phased array which is designed, built and programmed to levitate particles of any material. A frame is also designed and built to hold a second acoustic array for the investigation of multi-sided acoustic levitation. The physical array is proven to levitate particles of up to 4.2 mm made of polystyrene. A playlist of videos can be seen of the physical array on YouTube where demonstrations of the different features and modes of the arrays can be found. Shortened URL: <https://goo.gl/TB7AM5>

Approximately 5000 lines of source code written for this project to simulate and characterise the acoustic traps and the software written to program and control the array boards, which is predominantly written in python, is available for use and can be accessed on GitHub. URL: <https://github.com/NiallMacD/Project-X>

The future opportunities for the use of this technology and further research potential are vast. The software that is written to characterise the acoustic traps could be used with another piece of software to optimise the layout and orientation of multiple array boards to find the strongest possible trap type with two or more arrays. Depending on the use case and with enough computational power, an appropriate search space of parameters could be created to allow an algorithm to automatically optimise all parameters affecting the trap strength to find the strongest possible trap with the given arrays.

Another fascinating use for this technology is for particle sorting and manipulation, using computer vision and particle simulation to predict particle moments and selectively trap certain particles. This would require extensive work into computer vision and real-time image characterisation and software development for automatic sorting of particles.

Merging spectroscopy measurements with liquids levitation could allow for spectra to be taken of samples without the use of a cuvette. This could eliminate any interference that is introduced by the cuvette material. Levitating liquids has been proven to be possible with multi-sided acoustic levitation or standing wave levitation and as demonstrated in the array optimisation section, two of the arrays built in this project would be able to levitate liquids up to a density of  $3150 \text{ kg/m}^3$  while being separated by 10 cm. Moving the arrays closer or by using larger or more powerful arrays it would be possible to levitate metals and even molten metals if the arrays were sufficiently cooled.

Using the methods described above, by levitating a known volume of a liquid and observing its evaporation over time, it would be possible to determine diffusion coefficients of different liquids. As they evaporate the sphere of liquid would shrink and with correlations from the initial known volume, the volume and surface area over time could be determined with images taken of the evaporating sample.

In Earth's gravity, it isn't possible to observe liquid droplet-droplet interactions in a controlled manner as they fall downwards when they are released. Water droplet physics and the interactions between multiple droplets could be investigated with the use of acoustic levitation where multiple droplets can be levitated and brought together at varying velocities to study how they interact and merge. It may also be possible that while levitating a droplet of liquid, with careful manipulation of the array, it would be possible to induce Surface waves to the droplet and therefore allow for mixing of solutions while they are being levitated. This may be possible by using a similar principle to the haptic feedback modes of the array where the power of the array is modulated at a frequency that induces audible sound at the focus point.

Investigation of the acoustic trap volume shape is limited and requires more work to understand the relationships between the acoustic trap volume shape and how they perform at trapping different types of particles. How steep an acoustic trap is compared to another can show how stable a particle would be in that trap. Stability is directly related to the trap strength, but it is possible that a weaker trap could be a more stable trap if it had steeper walls.

These fascinating topics and many others are unexplored and have the potential to be developed through research which could add considerably to the already exciting topic of ultrasonic acoustic levitation.

---

CHAPTER  
**SEVEN**

---

REFERENCES

- [1] A Ashkin and JM Dziedzic. “Optical trapping and manipulation of viruses and bacteria”. In: *Science* 235.4795 (1987), pp. 1517–1520. DOI: [10.1126/science.3547653](https://doi.org/10.1126/science.3547653).
- [2] D. Foresti et al. “Acoustophoretic contactless transport and handling of matter in air”. In: *Proceedings of the National Academy of Sciences* 110.31 (July 2013), pp. 12549–12554. DOI: [10.1073/pnas.1301860110](https://doi.org/10.1073/pnas.1301860110).
- [3] Asier Marzo et al. “Holographic acoustic elements for manipulation of levitated objects”. In: *Nature Communications* 6 (Oct. 2015), p. 8661.
- [4] M. A., T. C., and B. W. Drinkwater. “Ultraino: an Open Phased-Array System for Narrowband Airborne Ultrasound Transmission.” In: *IEEE Transactions on Ultrasonics, Ferroelectrics, and Frequency Control* PP.99 (2017), pp. 1–1.
- [5] Marco A. B. Andrade, Anne L. Bernassau, and Julio C. Adamowski. “Acoustic levitation of a large solid sphere”. In: *Applied Physics Letters* 109.4 (2016), p. 044101. DOI: [10.1063/1.4959862](https://doi.org/10.1063/1.4959862).
- [6] A. Marzo et al. “Realization of compact tractor beams using acoustic delay-lines”. In: *Applied Physics Letters* 110.1 (2017), p. 014102. DOI: [10.1063/1.4972407](https://doi.org/10.1063/1.4972407).
- [7] E. H. Brandt. “Acoustic physics Suspended by sound”. In: *Nature* 413.6855 (Nov. 2001), pp. 474–475. DOI: [10.1038/35097192](https://doi.org/10.1038/35097192).
- [8] C.R.P. Courtney et al. “Dexterous manipulation of microparticles using Bessel-function acoustic pressure fields”. In: *Applied Physics Letters* 102.12 (Mar. 2013). DOI: [10.1063/1.4798584](https://doi.org/10.1063/1.4798584).
- [9] S. T. Kang and C. K. Yeh. “Potential-well model in acoustic tweezers”. In: *IEEE Transactions on Ultrasonics, Ferroelectrics, and Frequency Control* 57.6 (June 2010), pp. 1451–1459. DOI: [10.1109/TUFFC.2010.1564](https://doi.org/10.1109/TUFFC.2010.1564).
- [10] Diane Dalecki et al. “Tactile perception of ultrasound”. In: *The Journal of the Acoustical Society of America* 97.5 (1995), pp. 3165–3170. DOI: [10.1121/1.411877](https://doi.org/10.1121/1.411877).

- [11] Tom Carter et al. “UltraHaptics: Multi-point Mid-air Haptic Feedback for Touch Surfaces”. In: *Proceedings of the 26th Annual ACM Symposium on User Interface Software and Technology*. UIST ’13. St. Andrews, Scotland, United Kingdom: ACM, 2013, pp. 505–514. DOI: 10.1145/2501988.2502018.
- [12] Yoichi Ochiai, Takayuki Hoshi, and Ippei Suzuki. “Holographic Whisper: Rendering Audible Sound Spots in Three-dimensional Space by Focusing Ultrasonic Waves”. In: *Proceedings of the 2017 CHI Conference on Human Factors in Computing Systems*. CHI ’17. Denver, Colorado, USA: ACM, 2017, pp. 4314–4325. DOI: 10.1145/3025453.3025989.
- [13] M. Perry. *Receiver communications for wireless power transfer*. US Patent 9,001,622. Apr. 2015.
- [14] E. H. Trinh. “Compact acoustic levitation device for studies in fluid dynamics and material science in the laboratory and microgravity”. In: *Review of Scientific Instruments* 56.11 (1985), pp. 2059–2065. DOI: 10.1063/1.1138419.
- [15] Duyang Zang et al. “Acoustic levitation of soap bubbles in air: Beyond the half-wavelength limit of sound”. In: *Applied Physics Letters* 110.12 (2017), p. 121602. DOI: 10.1063/1.4979087.
- [16] Stanley Gelfand Stanley A. Gelfand. *Hearing An Introduction to Psychological and Physiological Acoustics*. Ed. by Stanley Gelfand. Taylor & Francis, 2004.
- [17] H. T. O’Neil. “Theory of Focusing Radiators”. In: *The Journal of the Acoustical Society of America* 21.5 (1949), pp. 516–526. DOI: 10.1121/1.1906542.
- [18] R. S. Longhurst. *Geometrical and physical optics [by] R. S. Longhurst*. English. 3d ed. Longman [London], 1973, xviii, 677 p.
- [19] RS Components, RS Pro Ultrasonic Sensor. Accessed: 2018-01-03, url: <http://docs-europe.electrocomponents.com/webdocs/1584/0900766b81584993.pdf>.
- [20] Louis V. King. “On the Acoustic Radiation Pressure on Spheres”. In: *Proceedings of the Royal Society of London. Series A, Mathematical and Physical Sciences* (1934-1990) 147.861 (Nov. 1934), pp. 212–240.
- [21] Henrik Bruus. “Acoustofluidics 7: The acoustic radiation force on small particles”. In: *Lab Chip* 12 (6 2012), pp. 1014–1021. DOI: 10.1039/C2LC21068A.
- [22] L. P. Gor’kov. “On the Forces Acting on a Small Particle in an Acoustical Field in an Ideal Fluid”. In: *Soviet Physics Doklady* 6 (Mar. 1962), p. 773.
- [23] M. Barmatz and P. Collas. “Acoustic radiation potential on a sphere in plane, cylindrical, and spherical standing wave fields”. In: *The Journal of the Acoustical Society of America* 77.3 (1985), pp. 928–945. DOI: 10.1121/1.392061.

- 
- [24] Asier Marzo, Mihai Caleap, and Bruce W. Drinkwater. “Acoustic Virtual Vortices with Tunable Orbital Angular Momentum for Trapping of Mie Particles”. In: *Physical Review Letters* 120.4 (Jan. 2018). DOI: 10.1103/PhysRevLett.120.044301.
  - [25] W. J. Xie and B. Wei. “Parametric study of single-axis acoustic levitation”. In: *Applied Physics Letters* 79.6 (2001), pp. 881–883. DOI: 10.1063/1.1391398.
  - [26] Asier Marzo, Adrian Barnes, and Bruce W. Drinkwater. “TinyLev: A multi-emitter single-axis acoustic levitator”. In: *Review of Scientific Instruments* 88.8 (2017), p. 085105. DOI: 10.1063/1.4989995.
  - [27] *Expanded Polystyrene Technical Data*. Accessed: 2018-04-08, url: [http://www.thermalps.com.au/imagesDB/wysiwyg/TDS\\_ExpandedPolystyrene.pdf](http://www.thermalps.com.au/imagesDB/wysiwyg/TDS_ExpandedPolystyrene.pdf). 2018.
  - [28] *Acoustic Levitator*. Accessed: 2018-01-06, url: <http://www.instructables.com/id/Acoustic-Levitator/>.
  - [29] Marco A. B. Andrade, Nicolas Perez, and Julio C. Adamowski. “Particle manipulation by a non-resonant acoustic levitator”. In: *Applied Physics Letters* 106.1 (2015), p. 014101. DOI: 10.1063/1.4905130.
  - [30] Z Prime and Con Doolan. “A comparison of popular beamforming arrays”. In: *Proceedings of Acoustics* (Jan. 2013), pp. 151–157.
  - [31] Lenny Fukshansky. *Revisiting the hexagonal lattice: on optimal lattice circle packing*. Tech. rep. arXiv:0911.4106. Comments: 8 pages, 1 figure; to appear in Elemente der Mathematik. Elemente der Mathematik, Nov. 2009.
  - [32] Loup Verlet. “Computer Experiments on Classical Fluids. I. Thermodynamical Properties of Lennard-Jones Molecules”. In: *Phys. Rev.* 159 (1 July 1967), pp. 98–103. DOI: 10.1103/PhysRev.159.98.